University of Cincinnati

Date: 11/4/2016

I, Arian Houshmand, hereby submit this original work as part of the requirements for the degree of Master of Science in Mechanical Engineering.

It is entitled:

Multidisciplinary Dynamic System Design Optimization of Hybrid Electric Vehicle Powertrains

Student's name: **Arian Houshmand**

This work and its defense approved by:

Committee chair: Michael Alexander-Ramos, Ph.D.

Committee member: Manish Kumar, Ph.D.

Committee member: David Thompson, Ph.D.

22400

Multidisciplinary Dynamic System Design Optimization of Hybrid Electric Vehicle Powertrains

A thesis submitted to the
Graduate School
of the University of Cincinnati
in partial fulfillment of the
requirements of the degree of

Master of Science

in the Department of Mechanical and Materials Engineering
of the College of Engineering and Applied Sciences
by

Arian Houshmand

B.S. Sharif University of Technology
June 2014

Committee Chair: Michael Alexander-Ramos, Ph.D.

Abstract

The design of large-scale, complex systems such as plug-in hybrid electric vehicles (PHEVs) motivates the use of formal optimization methods from both multidisciplinary design optimization (MDO) and optimal control theory. Traditionally, MDO methods have been used to address the integrated design of engineering systems comprised of multiple, interacting components and/or disciplines for superior static system performance. Optimal control theory, on the other hand, is often used to select the best operation strategy of a given dynamic system for superior dynamic system performance. Although many times in practice the optimal design and control of such dynamic systems are addressed almost independently [7, 38, 48], this approach generally yields sub-optimal overall design solutions [4] . This is because the system architecture, or physical design, is inherently coupled with its operation strategy, or control design. Combined optimal design and control techniques, also known as co-design, can address this issue by using an integrated approach to enable superior design solutions for dynamic systems [45, 48]. This thesis focuses on the co-design of large-scale systems, specifically PHEVs based on simultaneous multidisciplinary dynamic system design optimization (MDSDO) methods using direct transcription (DT). In order to enable a simultaneous approach for optimizing the design and control of the PHEV, a toolbox was developed to design all the critical component of a PHEV powertrain including: electric motor, generator, engine, transmission, and high voltage battery. This toolbox takes the size related design variables as inputs and by using the embedded analytical equations, generates the output performance characteristics of each component. The MDSDO problem formulation is then solved using GPOPS-II [39],a DT-based MATLAB software for solving multiple-phase optimal control problems. DT-based simultaneous problem formulations in MDSDO has already been successfully used in moderate scale problems, however there has been very few attempts to implement this method on large-scale problems. The current study addresses this issue and examines the practicality of DT-based simultaneous problem formulations in MDSDO for large-scale, complex dynamic systems.

ACKNOWLEDGEMENTS

I would first like to thank my thesis advisor Dr. Michael Alexander-Ramos. The door to his office was always open whenever I ran into a trouble spot or had a question about my research or writing. He consistently allowed this thesis to be my own work, but steered me in the right direction whenever he thought I needed it. I really appreciate his time for scrutinizing every aspect of my research and guiding me towards better solutions.

Besides my advisor, I would like to thank the rest of my thesis committee: Dr. David Thompson, and Dr. Manish Kumar for taking the time from their busy schedules to give me the much needed advise and direction to complete this project.

My sincerely thanks goes to Dr. Anil Rao, who provided me an opportunity to understand the mathematical aspects of my problem better. He helped me through my codes line by line, when I was trying to use their software (GPOPS-II), and spent hours guiding me through the right direction to perform my study. I really enjoyed talking with him about my project. I would say, without his precious support it would not be possible to conduct this research.

A special thanks to my family. Words cannot express how grateful I am to my father, and mother for all of their supports and sacrifices they have made on my behalf. I would also like to thank all of my friends who encouraged me towards my goals.

November, 2016

TABLE OF CONTENTS

LIST OF FIGURES

LIST OF TABLES

Nomenclature

a	rotor insulation ratio	
A_{cu}	copper cross sectional area	$[m^2]$
A_{fr}	vehicle frontal area	$[m^2]$
C_d	vehicle's air drag coefficient	
CR	compression ratio	
D_b	piston bore diameter	[m]
D_{end}	mean diameter of the end winding	[m]
D_{ri}	rotor inner diameter	[m]
D_{si}	stator inner diameter	[m]
D_{so}	stator outer diameter	[m]
F	internal reaction force between the sun and planet gears	[N]
F_{roll}	rolling resistance force	[N]
FR	fuel rate	[g/s]
g	acceleration of gravity	
g'	effective radial airgap	[m]
g_{mech}	mechanical radial airgap	[m]
h_m	magnet thickness	[m]
I	current	[A]
I_c	rated stator current	[A]
I_d	stator d-axis current	[A]
I_q	stator q-axis current	[A]
J_e	engine rotational inertia	$[kg.m^2]$

J_g	generator rotational inertia	$[kg.m^2]$
J_m	motor rotational inertia	$[kg.m^2]$
J_{rotor}	rotor moment of inertia	$[kg.m^2]$
J_w	wheel rotational inertia	$[kg.m^2]$
K	final drive ratio	
$k_{\omega 1}$	fundamental winding factor	
k_{cr}	Carter's airgap extension factor	
k_{cr}	Carter's coefficient considering the rotor slotting	
k_{cs}	Carter's coefficient considering the stator slotting	
k_{d1}	fundamental distribution factor	
k_{p1}	fundamental chord factor	
k_{s1}	fundamental skew factor	
l	stack length	[m]
$L(.)$	Lagrangian term	
L_1	stator leakage inductance	[H]
l_1	Height of stator tooth tip	[m]
l_2	Height of slot wedge	[m]
l_3	Height of slot wedge from wedge to slot bottom	[m]
L_{con}	total length of conductors	[m]
L_{dm}	magnetising d-axis synchronous inductance	[H]
L_d	d-axis synchronous inductance	[H]
L_{End}	end-winding leakage inductance	[H]
l_m	magnet length	[m]
$L_{OneTurn}$	the inductance of one turn of diameter D	[H]

L_{qm}	magnetising q-axis synchronous inductance	[H]
L_q	q-axis synchronous inductance:L_{qm}+L_1	[H]
L_{slt}	stator slot-leakage inductance	[H]
l_{st}	stroke length	[m]
LHV	lower heat value of the fuel	[kJ/g]
m_{batt}	battery mass	[kg]
$m_{chassis}$	chassis mass	[kg]
m_{eng}	engine mass	[kg]
m_{gen}	generator mass	[kg]
m_{motor}	electric motor mass	[kg]
M_{pm}	mass of permanent magnet	[kg]
m_p	number of phases of the electric machine	
M_{rc}	mass of rotor core	[kg]
M_{sc}	mass of stator core	[kg]
M_{st}	mass of stator teeth	[kg]
M_{sw}	mass of stator winding	[kg]
m_{veh}	vehicle mass	[kg]
MLT	mean length per turn	[m]
MLT_{end}	mean length of stator winding	[m]
MLT_{stack}	mean length of stator	[m]
N_{coil}	number of coils	
n_{cyl}	number of engine cylinders	
N_{ph}	number of series turns per phase	
N_{pm}	number of magnets	

N_p	number of parallel cells in the battery pack	
N_{sine}	number of effective sine-distributed turns per phase	
N_{slot}	number of slots	
N_s	number of series cells in the battery pack	
NSH	number of strands per phase	
p	number of pole pairs	
P_{batt}	battery power	[W]
P_{demand}	power demand at wheels	[W]
P_e	electic motor total power	[W]
P_F	fuel power	[kW]
P_m	electric motor output power (per phase)	[W]
P_{s1}	permeance of the slot section closest to the airgap	
P_{s2}	permeance of the inside of the tang	
P_{s3}	permeance of the main body	
P_s	slot permeance ratio	
Q	battery capacity	[A-h]
q	number of slots per pole per phase	
R	number of teeth on the ring gear	
R_1	stator inner radius	[m]
r_1	rotor radius	[m]
r_a	half the slot opening	[m]
R_i	battery internal resistance	[Ω]
r_{tire}	tire radius	[m]
S	number of teeth on the sun gear	

$SlotD$	slot depth measured from airgap	[m]
T_{co}	number of turns per coil	
t_F	length of the time horizon	[s]
$u(t)$	control input trajectory	
V	voltage	[V]
v	speed of the vehicle	[m/s]
V_c	rated phase voltage	[V]
V_{dis}	engine displacement	[liter]
V_d	d-axis voltage	[V]
V_{oc}	battery open circuit voltage	[V]
V_q	q-axis voltage	[V]
V_{veh}	vehicle speed	[km/h]
w_1	Stator slot opening at the slot tip	[m]
w_2	Stator slot opening at the slot wedge	[m]
w_3	Stator slot opening at the bottom of the wedge	[m]
W_d	bare copper wire diameter	[m]
w_m	magnet width	[m]
w_s	slot opening width	[m]
w_{tb}	tooth width at base	[m]
w_t	tooth width	[m]
$x(t)$	state variable trajectory	
X_{end}	end-turn leakage adjusment factor	
ϵ	winding chording angle	[deg]
η_{IT}	indicated thermal efficiency	

γ	electrical current-angle between I and q-axis	[deg]
γ_p	electrical slot pitch angle	[deg]
γ_m	maximum torque per ampere current angle	[deg]
κ	heat capacity ratio	
μ	rolling friction coefficient	
ω_m	rotational speed of the electric motor	[rad/s]
ω_b	base speed	[rad/s]
ω_e	engine speed	[rad/s]
ω_g	generator speed	[rad/s]
$\omega_{b-mg-elec}$	electrical base speed for motor and generator (rad/s)	
ω_{max}	maximum rotational speed (rad/s)	
$\omega_{max-mg-elec}$	maximum electricl rotational speed (motor/generator)(rad/s)	
$\psi(.)$	Mayer term	
ψ_m	flux-linkage due to magnets (Vs)	
ρ	air density	$[kgm^{-3}]$
ρ_{cu}	copper resistivity	[ohm meter]
ρ_{cu}	mass density of copper	$[\frac{kg}{m^3}]$
ρ_{pm}	mass density of permanent magnet	$[\frac{kg}{m^3}]$
ρ_s	mass density of steel	$[\frac{kg}{m^3}]$
σ	Carter's coefficient	
σ_o	Carter's coefficient for open slots	
σ_{sc}	Carter's coefficient for semi-closed slots	
τ_{demand}	torque demand at wheels	[Nm]
τ_e	engine torque	[Nm]

τ_k	rated torque of the electric motor	[Nm]
τ_m	electic motor torque (per phase)	[Nm]
$\tau_{mg-elec}$	electrical torque of motor/generator	[rad/s]

Chapter 1: INTRODUCTION

The design of large-scale, complex systems such as plug-in hybrid electric vehicles (PHEVs) motivates the use of formal optimization methods from both multidisciplinary design optimization (MDO) and optimal control theory. Traditionally, engineers use a hierarchical approach for designing the complex systems. In this approach, the physical design of the system is decided first, then control engineers design the optimal control strategies which are capable of optimizing the overall performance of the system. However, this procedure generally yields sub-optimal overall design solutions [4], due to the intrinsic coupling of system architecture, or physical design to its operation strategy, or control design. Combined optimal design and control techniques, also known as co-design, addresses this issue by considering both the design and control aspects of the system in the design process [45, 48]. Co-design can be compared to design for manufacturing (DFM) [4]. In other words, the coupling between system design and control is comparable to product design and manufacturing. The traditional approach for both is hierarchical which generally yields sub-optimal solutions and designs for the problem. Unlike the traditional approaches, co-design and DFM take advantage of an integrated approach, considering all the aspects of the system design in each stage of the product development. This simultaneous approach in co-design problems can ensure a truly optimal system solution for dynamic systems and it becomes even more critical for large scale systems.

This thesis is focused on the co-design of large-scale systems, specifically plug-in hybrid electric vehicles (PHEVS). A new branch of multidisciplinary design optimization (MDO) theory known as multidisciplinary dynamic system design optimization (MDSDO) which can address the limitations of the traditional co-design approach is used in this work. A common and efficient approach to handle simultaneous co-design problem formulations from an MDSDO perspective is to use direct transcription (DT) techniques from optimal control theory to parameterize infinite-dimensional input control decision variables and their associated constraints [4]. Despite the success of DT-based simultaneous problem formulations in MDSDO for moderate-scale, complex dynamic systems, there have been very few studies to date that extend such methods to large scale, complex dynamic systems. This thesis examines the practicality of DT-based simultaneous problem formulations in MDSDO for large-scale, complex dynamic systems.

The PHEV powertrain architecture is the case study chosen in this thesis to examine the practicality of DT-based simultaneous problem formulations in MDSDO for large-scale, complex dynamic systems. In particular, this research investigates the combined design and supervisory control of a complete PHEV powertrain to minimize the fuel cost of the vehicle. Plug-in hybrid electric vehicles are hybrid vehicles that have a battery that can be charged using an external source of electric power and thus can improve fuel economy and reduce emission significantly compared to non-plug-in hybrid electric vehicles and conventional internal combustion engine (ICE) vehicles [47]. Due to the coupling between the control strategies and design of the components in a PHEV, it is necessary to study the effects of both the

design and control of the system on the overall fuel efficiency for having the optimal design of the system. The general approach that has been used in the literature to optimize the design of the PHEV powertrain, is using the experimental driven performance maps of the components and some scaling factors to scale the performance for different designs. In other words, instead of changing the physical design of the system, a scaling factor is chosen that can shift the performance maps to the desirable regions. Although this is a straightforward approach, it has some limitations. Scaling factors only work within a limited range and do not imply anything about how the actual design parameters should change. These limitations prevent us from obtaining meaningful design parameters for the system. To overcome this issue, in this work, a toolbox is developed that generates the performance characteristics of important components of the PHEV powertrain using analytical equations based on their design parameters. This toolbox generates the performance models for the electric motor, generator, high-voltage battery and engine by having up to four design parameters as the input for each model. After developing the toolbox to generate the output performance of the vehicle based on the design parameters, we had to come up with a mathematical strategy to solve the co-design problem formulations from an MDSDO perspective. GPOPS-II [39],a DT-based MATLAB software for solving multiple-phase optimal control problems, was implemented to solve the simultaneous problem formulation.

Two MDSDO studies for a power-split PHEV powertrain have been performed in this thesis. The first study investigates the component sizing of the high-voltage battery along with the supervisory control of the engine, electric motor, and generator such that the overall system energy cost is minimized and the system performance-related constraints are satisfied. In the second study, we have investigated the component sizing of the complete powertrain, including the engine, electric motor, generator, transmission, and high-voltage battery, along with the supervisory control of the engine and electric motor for the same system decision objectives and constraints. Note that the component models used in both studies contains sufficient details such that their sizing is described by up to four decision variables (four design variables for motor and generator, three for engine, and two for battery). Also, in both studies a DT-based simultaneous problem formulation was used to facilitate efficient solution strategies. The results from these two studies were compared to one another to determine the extent to which their optimal design solutions differ since previous work on a similar problem suggested that only battery design was significant in such co-design problems [24, 32, 38]. Hence, we have examined the importance of including the entire propulsion system for the co-design problem while fully demonstrating the capability of MDSDO methods for large-scale, complex system design problems.

Chapter 2: BACKGROUND

2.1 Combined Design and Control

Traditionally, designers use a sequential process for design and optimization of the systems. In this approach, the plant is designed and the design variables are being optimized to satisfy the objective function; then an optimal control strategy is chosen [7, 48]. In other words, the optimal control and optimal design are addressed independently. The aforementioned approach, generally yields to sub-optimal overall design solutions [4]. This is because the system architecture, or physical design, is inherently coupled with its operation strategy, or control design. Combined optimal design and control techniques, also known as co-design, can address this issue by using an integrated approach [19] that enables superior design solutions for dynamic systems [45, 48]. Co-design problems have been historically classified into two broad categories known as simultaneous and nested formulations [4, 43]. Simultaneous problem formulations solve a single optimization problem for a comprehensive (physical architecture and control) dynamic system design objective and associated constraints. Nested problem formulations, however, solve two optimization problems for a comprehensive dynamic system design objective by embedding an optimal control problem within an optimal physical system design problem [18]. Both of these approaches have been theoretically proven to yield the combined optimal design and control solution of an integrated dynamic system [4].

2.1.1 Simultaneous Problem Formulation

The simultaneous formulation ,also known as All-at-Once (AAO) [26], solves a single optimization problem for a comprehensive dynamic system objective and associated constraints2.1.

$$\min_{d,x(t),u(t)} \phi(d, x(t), u(t), t) \tag{2.1}$$

subject to:

$$g(d, x(t), u(t)) \leq 0$$

$$h(d, x(t), u(t)) = 0$$

$$\dot{x}(t) - f(d, x(t), u(t), t) = 0$$

where $\phi(.)$ is the dynamic system objective function, $g(.)$ is the the vector of system inequality constraints,$h(.)$ is the vector of equality constraints, $f(.)$ is the dynamic system constraint, d is the vector of design variables, $x(t)$ is the vector of state decision variables, $u(t)$ is the vector of input decision variables, and t is time.

For a practical rendering of a simultaneous co-design problem, the infinite-dimensional decision variables $x(t)$ and

$u(t)$ must be parameterized directly or indirectly. Traditionally, parameterization is performed indirectly by assuming a feedback control structure and using control gains as decision variables. Some of the advantages of simultaneous co-design problem formulations are the simplicity of the problem formulation as well as its computational efficiency. Moreover, the accuracy of the original control related decision variables is preserved. On the other hand, the exploration of alternative optimal control solutions is limited due to the assumption of a feedback control system topology.

2.1.2 Nested Problem Formulation

The nested problem formulation solves two optimization problems, an embedded optimal control problem within an optimal design problem, for a comprehensive dynamic system objective and associated constraints (2.2).

$$\min_{d} \phi_*(d) = \begin{cases} \min\limits_{x(t),u(t)} \phi(d, x(t), u(t), t) \\ s.t \quad g(d, x(t), u(t)) \leq 0 \\ \qquad h(d, x(t), u(t)) = 0 \\ \qquad \dot{x}(t) - f(d, x(t), u(t), t) = 0 \end{cases} \tag{2.2}$$

$$\begin{aligned} s.t \quad & g_d(d) \leq 0 \\ & h_d(d) = 0 \end{aligned}$$

where $\phi_*(.)$ is the optimal dynamic system objective value function, $g_d(.)$ is the vector of design inequality constraints, and $h_d(.)$ is the vector of design equality constraints.

In the nested formulation, the infinite dimensional decision variables are decoupled from the design variables, which enables the nested co-design problem to be solved [4]. The embedded optimal control problem is usually solved using indirect methods, closed form solutions, or dynamic programming [38]. The nested co-design problem formulation has the following advantages:

- Any well-known optimal control method can be used to determine the optimal controls-related decision variables.
- The accuracy of the controls-related decision variables may be preserved.

Apart from the mentioned advantages of this method, it can be complex and computationally expensive.

In the traditional co-design problems, the system objective is considered as a sum of design-oriented and control-oriented objective functions, thus limiting the scope of the optimization model. Moreover, there is a strong control-oriented focus in the existing co-design methods which consequently reduces the design optimization problem to a design requirements optimization problem. As a result, the scope of the problems that can be solved using this method

are limited to those that require knowledge of the control system topology and/or are completely efficient [5].

2.2 MDSDO

Multidisciplinary dynamic system design optimization (MDSDO) [3] is a relatively new branch of multidisciplinary design optimization (MDO) which can improve the traditional co-design approach. MDSDO theory is based on both optimal control and MDO theory and thus it can take advantage of many of their associated practical solution techniques [3]. The focus in MDSDO is on the systems where the evolution of the state over time is largely dependent on the value or functionality of the system [4].

MDSDO models can be used in analyzing the existing systems and predicting the system behavior given the current input specifications, as well as identifying the system specifications for designing a system that produces the desired output behaviors. Physical and control system design affects the overall behavior of an active controlled dynamic system. Even though the physical-system and control-system behaviors significantly affect each other and are coupled to each other, they are often inspected separately. MDSDO addresses the physical and control system design and optimization simultaneously. The MDSDO framework and using the simultaneous problem formulation motivates the use of direct transcription (DT) methods from optimal control theory for the parameterization of $x(t)$ and $u(t)$ and their associated constraints [3,4,6]. DT is a discretize then optimize method. The most popular MDSDO simultaneous formulation using direct transcription (DT) [4]2.3:

$$\begin{cases} & \min\limits_{d,x(t),u(t)} \phi(d,x(t),u(t),t) \\ s.t & g(d,x(t),u(t)) \leq 0 \\ & h(d,x(t),u(t)) = 0 \\ & \dot{x}(t) - f(d,x(t),u(t),t) = 0 \end{cases} \rightarrow \begin{cases} & \min\limits_{d,X,U} \phi(d,X,U) \\ s.t & g(d,X,U) \leq 0 \\ & h(d,X,U) = 0 \\ & \zeta(d,X,U) = 0 \end{cases} \tag{2.3}$$

where $\zeta(.)$ is the vector of defect (discretized dynamic system) constraints, X is the matrix of discretized state decision variables, and U is the matrix of discretized input decision variables.

DT-based simultaneous problem has the following advantageous:

- The exploration of alternative optimal control solutions is enabled since there are no assumptions imposed regarding the control system topology.
- The problem formulation is simple and efficient relative to most nested formulations.

On the other hand, DT-based simultaneous problem has the following limitations:

- Because of the problem discretization some degree of accuracy is lost in the optimal control solutuion.

- The generation of explicit dynamic constraints for DT can be cumbersome.

DT-based simultaneous problem formulations have been successfully applied to many moderate scale problems [3, 6], however, due to the aforementioned limitations, there have been very few attempts to apply this method on large scale problems. As a result, we have been motivated to apply this method on a large scale system (PHEV powertrain) in this work.

2.3 Co-Design of HEVs

Many studies have been focused on the co-design of hybrid electric vehicles (HEV). Patil [37, 38] has performed a co-design study on a PHEV architecture. The main focus of his work is on the optimal control of the PHEV using dynamic programming. He has also used a nested formulation to optimize only the design of the high voltage battery and find the optimal control strategy for the PHEV. Assanis et al. [7]used a nested approach to size the engine of a HEV based on empirical data and scaling the design variables. In this work, the design variables were limited to a single component of the powertrain, and the design changes were based on some scaling factors of the design variables. A more involved study was done by Egardt et al. [15]. In this study, the authors performed a co-design study for the complete powertrain of a PHEV using convex optimization. The authors used a simultaneous formulation in their study, and also took advantage of scaling factors for changing their design variables. In this study, the models were approximated by convex functions and then optimized. This approach guarantees a global optimal solution, however it loses the accuracy due to the convex approximation. Murgovski et al. [33]also used a convex approach for simultaneous optimization of battery sizing and power management of a PHEV. Perez et al. [40] used DT-based problem formulations in optimal control for optimal power management of a HEV. In all of the studies mentioned, the authors used scaling factors to change their designs using the known performance curves from commercially available software. This approach only gives us an idea on how much the design variables should change, however it does not provide us with any specific information on how much each design variable should change. As a result, a detailed analytical model is needed for each component such that the performance of the component is a function of its design variables. Having such a model, we can find a more detailed description for changes in design. As a result, in this thesis we first developed an analytical model for important components of the powertrain and then used the MDSDO approach using direct transcription (DT) to solve the co-design of a PHEV powertrain. The uniqueness of this work is due to the use of the MDSDO approach, which balances the importance of design and control in a more equitable way, and also the use of the simultaneous problem formulation.

Chapter 3: PHEV MODELING

Hybrid electric vehicles (HEV) are becoming increasingly common as automakers make use of alternative energy storage systems to improve vehicle performance and efficiency, and to reduce their environmental impact [16]. Plug-in hybrid electric vehicles (PHEVs) are HEVs with a battery that can be charged using an external source of electric power, thus improving fuel economy and reducing emissions significantly compared to other HEVs and conventional internal combustion engine (ICE) vehicles [47]. The main components in a PHEV are the engine, motor/generator unit(s), high-voltage battery, and transmission.. PHEVs also have three different architectures: series, parallel, and power split. The configurations of these architectures is shown in Figure 3.1 [25].

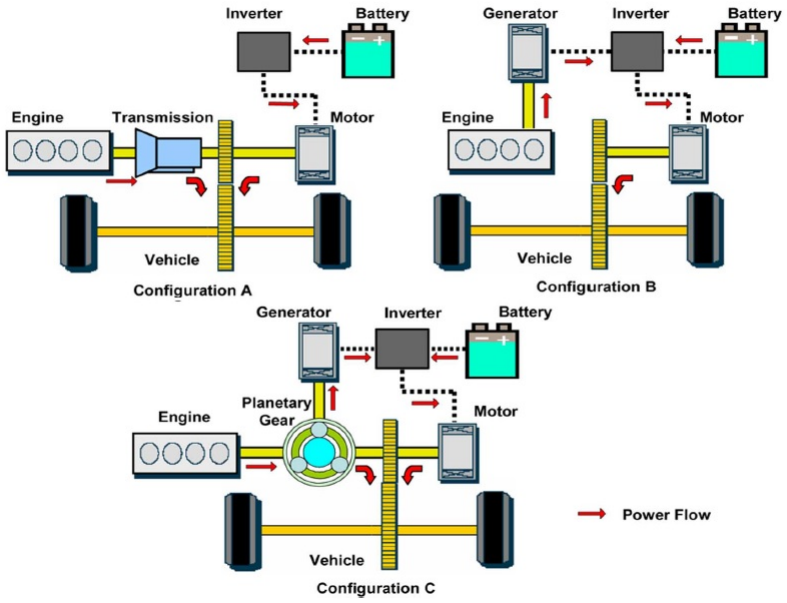

Figure 3.1: Hybrid vehicle configurations: (A) parallel; (B) series; and (C) power-split (parallel/series). Diagram adapted from [25].

In a series PHEV, the engine does not drive the vehicle directly. In these types of vehicles, the output power of the engine goes to the generator and the generated electricity goes into the motor as well as the battery. Hence, the motor power is supplied from either the generator or the battery. The motor is connected to the wheels through the transmission and thus drives the vehicle. In a series configuration, since the engine operation is independent of the vehicle's speed , it can work efficiently near its optimal working conditions. The parallel configuration, however, includes both an electrical and a mechanical power path. Note that the vehicle can be driven independently or collaboratively by each of these paths. The downside of this configuration is that often an individual unit acts as both motor and generator which complicates the control strategy [25] . The power-split configuration, which is the most sophisticated architecture, is a combination of both the series and parallel configurations. It uses a power split device, typically in

the form of a planetary gear system, to couple the engine, generator, and electric motor within the powertrain system. A schematic of the power-split configuration is shown in Figure3.2 where M/G1 is the generator and M/G2 is the motor.

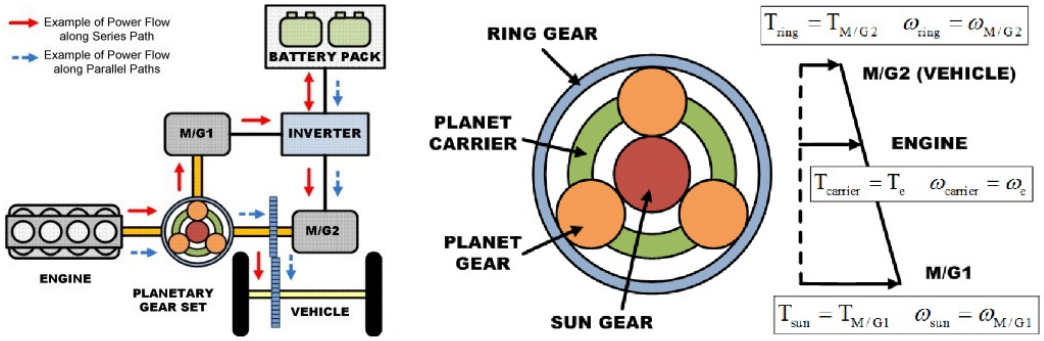

Figure 3.2: The single mode power-split hybrid architecture. Diagram adapted from [34] (M/G1 is generator and MG/2 is motor)

3.1 Powertrain Model

The powertrain model used in this thesis is based on a single-mode, power-split PHEV architecture that is similar to that of the MY2004 Toyota Prius. It consists of three control input variables and three state variables. The control input variables include the engine torque (τ_e), the electric motor torque (τ_m), and the electric generator torque (τ_g). The state variables include the engine rotational speed (ω_e), the electric motor rotational speed (ω_m), and the battery state of charge (SOC). Note that due to the nature of these variables, the powertrain model is governed by both mechanical and electrical dynamic equations. To derive the mechanical dynamic equations that govern the PHEV powertrain model, the vehicle road load (F_{road}) must first be defined:

$$F_{road} = F_{roll} + F_{drag} \tag{3.1}$$

In the above, F_{roll} is the rolling resistance and is given by:

$$F_{roll} = \mu m_{veh} g \tag{3.2}$$

$$m_{veh} = m_{eng} + m_{gen} + m_{motor} + m_{batt} + m_{chassis} \tag{3.3}$$

where μ is the rolling friction coefficient, $m_{veh}$is the vehicle mass, m_{eng} is the engine mass, m_{gen} is the generator mass, m_{motor} is the motor mass, m_{batt} is the battery mass, $m_{chassis}$ is the chassis mass, and g is the acceleration due

to gravity. The drag force is defined as:

$$F_{drag} = 0.5\rho A_{fr} C_d v^2 = 0.5\rho A_{fr} C_d (\frac{\omega_m {r_{tire}}^2}{K}) \tag{3.4}$$

where ρ is the air density, A_{fr} is the vehicle frontal area , C_d is the vehicle air drag coefficient, v is the speed of the vehicle , r_{tire} is the tire radius s, and K is the final drive ratio.

Recall that the engine, generator, and motor are all connected together via the planetary gear set (Figure 3.2). For this specific architecture, Liu and Peng [25]have shown that the road load and rotational speeds can be related to each other using the following :

$$\begin{bmatrix} J_e & 0 & 0 & R+S \\ 0 & J_g & 0 & -S \\ 0 & 0 & J'_m & -R \\ -(R+S) & S & R & 0 \end{bmatrix} \begin{bmatrix} \dot{\omega_e} \\ \dot{\omega_g} \\ \dot{\omega_m} \\ F \end{bmatrix} = \begin{bmatrix} \tau_e \\ \tau_g \\ \tau'_m \\ 0 \end{bmatrix} \tag{3.5}$$

$$J'_m = J_m + (J_w + m_{veh} r_{tire}^2)/K^2 \tag{3.6}$$

$$\tau'_m = \tau_m - F_{road} r_{tire}/K \tag{3.7}$$

In the above, J_e is the rotational inertia of the engine, J_g is the rotational inertia of the generator, J_m is the rotational inertia of the motor, J_w is the rotational inertia of the wheel, R is the number of teeth on the ring gear, S is the number of teeth on the sun gear, F is the internal reaction force between the sun and planet gears, K is the final drive ratio, $\omega_g$is the generator rotational speed, and r_{tire} is the tire radius. Note that the dependencies between the component speeds in the planetary gear set are governed by Eqn. 3.8:

$$\omega_g = (1 + \frac{R}{S})\omega_e - \frac{R}{S}\omega_m \tag{3.8}$$

Finally, the state-space equations used for this study can be obtained by using the final matrix equation in Eqn. 3.5 to eliminate F and Eqn. 3.8 to eliminate $\dot{\omega}_g$ as:

$$\dot{\omega}_m = \frac{\tau_m - \frac{r_{tire}}{K}(\mu m_{veh} g + 0.5\rho A_{fr} C_d (\frac{\omega_m r_{tire}}{2})^2) + A\tau_e + \frac{A(R+S)-R}{S}\tau_g}{J'_m + J_g(\frac{R}{S})^2 - AJ_g\frac{R(R+S)}{S^2}} \tag{3.9}$$

$$A = \frac{J_g R(R+S)}{S^2(J_e + J_g(\frac{R+S}{S})^2)} \tag{3.10}$$

$$\dot{\omega}_e = \frac{\tau_e + \frac{R+S}{S}\tau_g + J_g\frac{R}{S^2}(R+S)\dot{\omega}_m}{J_e + J_g(\frac{R+S}{S})^2} \tag{3.11}$$

The electrical dynamics governing the PHEV powertrain model are directly related to the battery dynamics. Therefore, a widely-used battery dynamic model developed by Mierlo et al. [52] is implemented. This model assumes that the battery dynamics can be captured through its open circuit voltage, internal resistance, and capacity. Although a full model derivation will be discussed in Section 3.4, the resultant state-space equation is defined as:

$$\dot{SOC} = \frac{V_{oc}(SOC) - \sqrt{V_{oc}^2(SOC) - 4P_{batt}R_i(SOC)}}{2QR_i(SOC)} \tag{3.12}$$

In this equation, P_{batt} is the battery power, Q is the battery capacity, and $V_{oc}(SOC)$ and $R_i(SOC)$ are the battery open circuit voltage and battery internal resistance, respectively, both of which are functions of SOC. Finally, note that P_{batt} is related to the motor and generator power through the following equation:

$$P_{batt} = P_{MG1} + P_{MG2} \tag{3.13}$$

where $P_{MG1}$and P_{MG2} are the power demand of generator and motor respectively.

The values of the fixed parameters described in this section are listed in Table. 3.1.

Table 3.1: Fixed parameters of the road-load model

Parameter	Value
rolling friction coefficient (μ)	0.007
acceleration due to gravity (g)	9.8 (m/s^2)
air density (ρ)	1.225 (kgm^{-3})
vehicle frontal area (A_{fr})	1.746 (m^2)
rotational inertia of the wheel (J_w)	0.74 (kg/m^2)
tire radius (r_{tire})	0.282 (m)
number of teeth on the ring gear (R)	78
number of teeth on the sun gear (S)	30
chassis mass($m_{chassis}$)	900 (kg)

3.2 Engine Model

Several empirical [20] , thermodynamic, and fluid dynamic models have been developed to understand the operation of the internal combustion engine. The empirical models are dependent on engine characteristics and cannot be extended to a general engine. Attempts have been made to scale the empirical models for a general engine, but such activities have required a great amount of engine test data [44]. The thermodynamics models consist of zero- or quasi-dimensional models. Zero-dimensional models are not accurately sensitive to the cylinder dimensions and the sizing parameters are considered as mean values. Fluid flow patterns cannot be evaluated using this model, but due to the speed and computational efficiency of this model, it is often used [46]. Quasi-dimensional models are rigorously based on thermodynamic models. They are used to find the effects of the flow rate, fuel chemical composition and chamber

dimensions on the overall performance of the engine [1, 46]. Developing quasi-dimensional models requires knowing a great deal of knowledge regarding sophisticated thermodynamical theories which is beyond the scope of this thesis. Fluid dynamic models use CFD models and are derived from the Navier-Stokes equations.. These type of models can predict the flow characteristics as well as the combustion chamber dimensions in detail [46]. CFD models are based on rigorous finite element models and are not computationally efficient to use in this study. Blumberg [10] provides a detailed survey of the phenomenological models developed based on empirical relationships. These methods are based heavily on combustion and consider the geometry of the combustion chamber in detail, which complicates the model beyond the requirements of this study. Methods proposed by Syed *et. al [50]* consider the engine as a first or second order system with coefficients that are experimentally determined. Although this predicts the response of the system accurately, it can't be implemented as the coefficients are dependent on the engine design variables. Therefore, the zeroth order method prescribed by Matthews *et. al* [27] combined with a model suggested by Nam et. al [35] has been implemented to calculate the maximum torque curve and the fuel consumption rate of a naturally-aspirated Otto cycle engine based on an appropriate selection of physically meaningful design variables.

3.2.1 Maximum Torque Curve model

The engine model is developed as a zeroth order model for the Otto-Cycle with compression ratio CR,stroke length l_{st}, and piston bore diameter D_b as the design variables. The first step in developing the engine model is calculating the maximum allowable torque as a function of ω_e. For this purpose we use a scalable model suggested by [35]. Before showing the equations we need to calculate the engine displacement (V_{dis}) as follow:

$$V_{dis} = n_{cyl}\frac{\pi}{4}D_b^2 l_{st} \tag{3.14}$$

where n_{cyl} is the number of cylinders in the engine. In [35] the author suggests a simple 7^{th} order polynomial to estimate the maximum bmep as:

$$bmep_{max} = 2\pi(a_0 + a_1\omega_e + a_2\omega_e^2 + a_3\omega_e^3 + a_4\omega_e^4 + a_5\omega_e^5 + a_6\omega_e^6 + a_7\omega_e^7) \tag{3.15}$$

In this equation. ω_e is the engine speed in rad/s and the coefficients are:

$$a_0 = -1200.51$$

$$a_1 = 298.934$$

$$a_2 = -17.5860$$

$$a_3 = 0.563420$$

$$a_4 = -.0104629$$

$$a_5 = 0.000113228$$

$$a_6 = -6.64513 * 10^{-7}$$

$$a_7 = 1.63097 * 10^{-9}$$

It follows that the max torque can be calculated as:

$$\tau_{e(max)} = \frac{bmep_{max} V_{dis}}{4\pi} \tag{3.16}$$

The maximum torque and power curves calculated for Toyota Prius engine based on the equation 3.15 is shown in Fig. 3.3b.

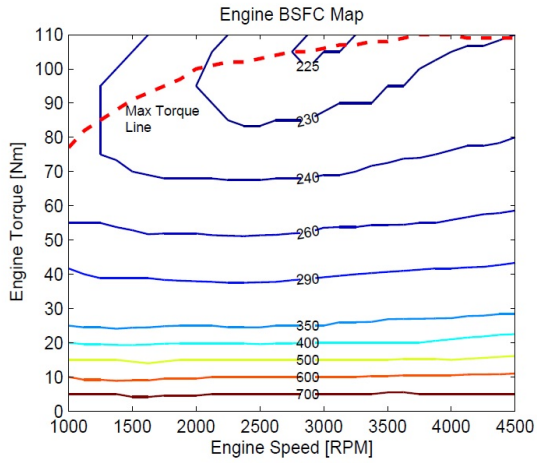

(a) Toyota Prius BSFC map [38]

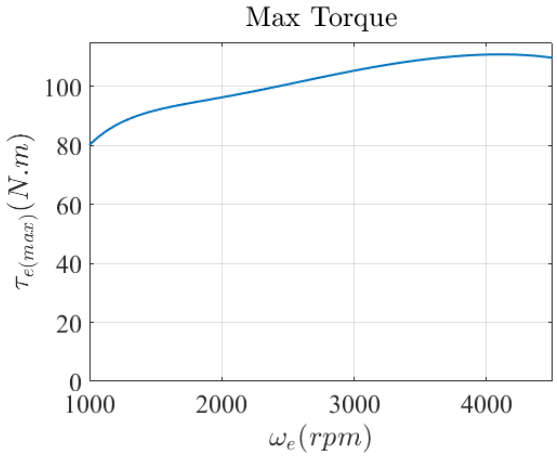

(b) Maximum torque curve for Toyota Prius engine based on the model

Figure 3.3: Comparison between the actual Toyota Prius max torque curve and the generated values by the model

3.2.2 Fuel Rate Consumption Model

The brake mean effective pressure in an internal combustion engine can be calculated as:

$$bmep = \frac{4\pi\tau_e}{V_{dis}} \tag{3.17}$$

Heywood [23] suggested the empirical equation 3.18 for engines with a displacement between 845 and 2000 cc to calculate the friction mean effective pressure (fmep) :

$$fmep(kpa) = 97 + 15(\frac{\omega_e}{1000}) + 5(\frac{\omega_e}{1000})^2 \tag{3.18}$$

The indicated mep (imep) is given by:

$$imep = bmep + fmep \tag{3.19}$$

Assuming the ideal *Otto Cycle,* the indicated thermal efficiency η_{IT} is given by:

$$\eta_{IT} = 1 - \frac{1}{CR^{\kappa-1}} \tag{3.20}$$

where κ is the heat capacity ratio. The mean effective pressure associated with the fuel is given by:

$$mep_{fuel} = \frac{imep}{\eta_{IT}} \tag{3.21}$$

The fuel power P_F can be calculated by:

$$P_F = \frac{2\pi mep_{fuel} V_{dis} \omega_e}{2000} \tag{3.22}$$

Finally, the fuel rate FR $[g/s]$ can be calculated by knowing the fuel power P_F and the lower heating value LHV of fuel:

$$FR = \frac{P_F}{LHV} \tag{3.23}$$

In Fig. 3.4a an output plot of the model is shown. In Fig. 3.4b engine fuel map of the Toyota Prius based on the experimental data is shown [55]. Comparing the map generated by the developed model and the experimental data, it is observed that even though we have a simplistic model, it has acceptable accuracy.

3.2.3 Engine Inertia Model

Due to the complexity of models for calculating the engine mass and moment of inertia, we used a simple approach to calculate these values. The engine mass is calculated by assuming a constant ratio between the maximum torque at 5000 rpm (maximum power of engine) and the engine mass as follow:

$$\frac{\tau_e(@5000rpm)}{m_{eng(nominal)}} = 0.6869 \tag{3.24}$$

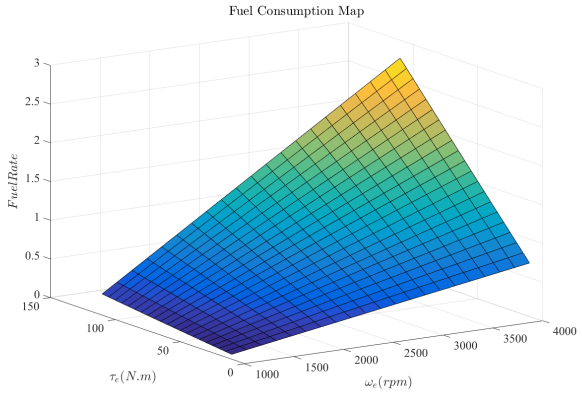

(a) Fuel consumption map generated by the Matlab code

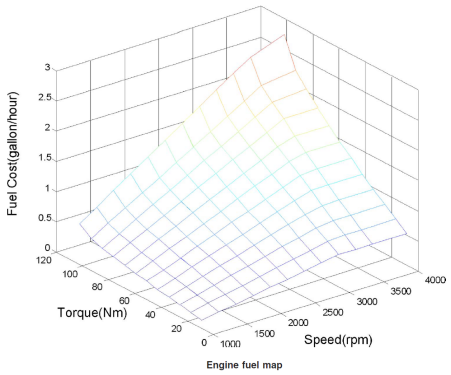

(b) Toyota Prius engine map (experimental)

Figure 3.4: Comparison of engine fuel consumption map. a) Map generated by the Matlba code b) Toyota Prius engine map (experimental) [55]

Hence the engine mass (m_{eng}) is given by:

$$m_{eng} = \frac{\tau_e(@5000rpm)}{0.6869} \tag{3.25}$$

Engine rotational inertia (J_e) is also calculated by assuming a constant ratio between engine mass and its rotational inertia as follow:

$$\frac{m_{eng(nominal)}}{J_{e(nominal)}} = 839 \tag{3.26}$$

$$J_e = \frac{m_{eng}}{839} \tag{3.27}$$

The engine parameters used in the Matlab code are shown in table 3.2

Table 3.2: Engine specifications used in Matlab code

Parameter	Value
Lower Heating Value of Fuel (LHV)	43.448 kJ/g
Specific Heat Ratio (κ)	1.5

3.3 Electric Machines

Electric machines are critical components within a PHEV powertrain that transform electrical power into mechanical power and vice versa. Note that when these machines are solely designed to convert electrical power into mechanical power, they are referred to as motors; conversely, when these machines are solely designed to convert mechanical power into electrical power, they are referred to as generators. Although permanent magnet (PM) machines, induction machines (IM), and switched reluctance (SR) machines are all reasonable options for vehicle propulsion applications,

PM machines are the most preferred due to their superior torque density [42].

There are two main types of PM machines: interior permanent magnet synchronous machines (IPMSMs) and surface permanent magnet synchronous machines (SPMSMs). Most automakers are interested in IPMSMs for electrified propulsion due to their relatively low price, reliable operation, and mature control techniques [51]. Therefore, in this study, the electric machine models that are used for the motor and generator are based on the IPMSM architecture.

Electric machines have limiting torque-speed characteristic as shown in Fig. 3.5. Traction motors usually have a constant torque range from the starting speed to the base speed. They also have a large constant power speed range (CPSR). The base speed ω_b is defined as "the speed at which the machine develops its continuous rated torque and power with rated inverter output voltage, the available DC link supply voltage and rated magnetic field in the air gap [42]. Base speed is approximately the speed at which the acceleration is completed and the torque starts to decrease as higher speed is achieved.

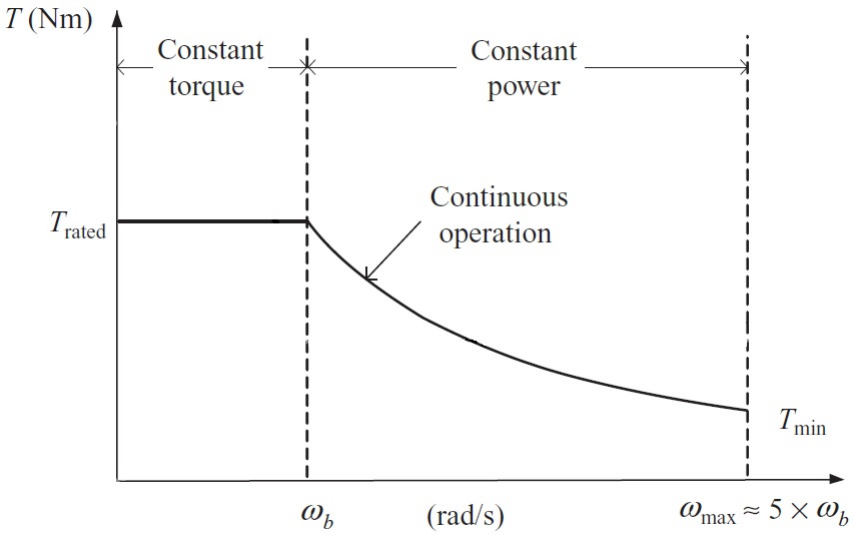

Figure 3.5: Limiting torque-speed characteristics of electric machines (assuming no mechanical losses)

Acceleration demand decreases as the electric machine reaches the desired speed. Maintaining the steady speed above the base speed, demands much lower torque than the maximum torque. Fast acceleration above the base speed requires higher power than the product of the rated torque and the base speed so we should compromise between the required maximum acceleration at high speed and motor power rating. Aerodynamic force is proportional to the speed squared and it becomes very large at high speeds. Consequently, a max speed, ω_{max}, is defined at which the motor cannot meet the torque demand above that value. The speed range at which the traction motor can deliver the acceleration limited to the power rating is specified by the ω_{max}/ω_bratio. Note that the maximum power of the machine remains constant between the speed range of $\omega_b$and ω_{max}due to the current and voltage limitations of the inverter and motor. This speed range is called the constant power speed range (CPSR=ω_{max}/ω_b). For clutchless

operations it has been found that the $CSPR \approx 5$ [42].

3.3.1 Maximum Torque and Electrical Power model:

The equivalent cicuit and phasor diagram of an IPMSM are shown in Fig. 3.6 and Fig. 3.7 respectively. The conventional per phase D-Q steady state equations for torque and voltage of an IPM machine, considering the stator resistance R_s, can be obtained from the Fig. 3.7 base on the work done by [49] as follows:

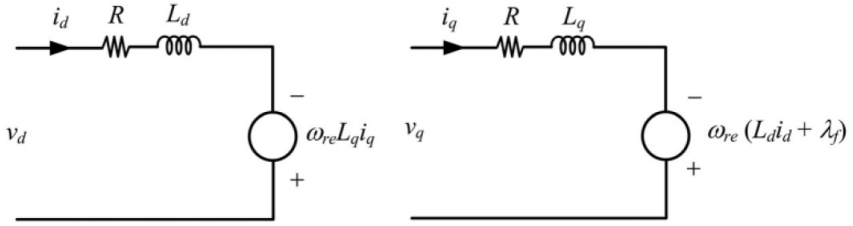

Figure 3.6: Circuit representation of an IPMSM in rotor d- and q-axes [42]

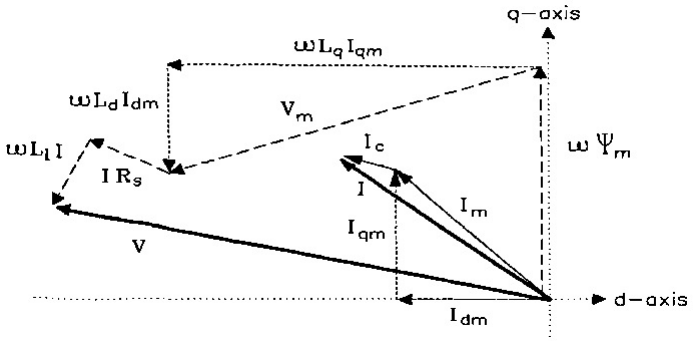

Figure 3.7: IPM phasor diagram [49]

$$V_d = R_s I_d - \omega L_d I_q \tag{3.28}$$

$$V_q = R_s I_q + \omega L_d I_d + \omega \psi_m \tag{3.29}$$

$$\tau_{mg-elec} = \psi_m I_q - (L_q - L_d) I_d I_q \tag{3.30}$$

where $\tau_{mg-elec}$ is the electrical torque of motor/generator and $\psi_m = I_c L_d$.

Defining $\xi = \frac{L_q}{L_d}$ and having $I_d = -Isin\gamma$ and $I_q = Icos\gamma$ from the above diagram we have:

$$V_d = R_s I_d - \omega L_d I cos\gamma \tag{3.31}$$

$$V_q = R_s I_q + \omega L_d I sin\gamma + \omega \psi_m \tag{3.32}$$

$$\tau_{mg-elec} = \psi_m I cos\gamma + 0.5(\xi - 1) L_d I^2 sin2\gamma \tag{3.33}$$

where:

$$I \leq I_c \tag{3.34}$$

$$V = \sqrt{V_d^2 + V_q^2} \leq V_c \tag{3.35}$$

The electrical speed corresponding to a given phase voltage V, phase current I, and current-angle γ can be found as:

$$\omega_{ele-mg} = \frac{-B \pm \sqrt{B^2 - 4AC}}{2A} \tag{3.36}$$

where:

$$A = K_d^2 + K_q^2 \tag{3.37}$$

$$B = 2R_s(-K_d I_d + K_q I_q) \tag{3.38}$$

$$C = R_s^2(I_d^2 + I_q^2) - V_c^2 \tag{3.39}$$

where R_s is the stator resistance, V_c is the rated voltage and:

$$K_d = L_q I_q \tag{3.40}$$

$$K_q = L_d I_d + \psi_m \tag{3.41}$$

In [49], two operation modes have been defined for an IPMSM. Mode I is in the speed range from zero to base speed ω_b, and Mode II is in the range from base speed $\omega_{b-mg-elec}$ to maximum speed $\omega_{max-mg-elec}$ for both motor and generator. In other words, Mode I is the constant torque range and Mode II is the constant power range. The maximum torque and corresponding rotational speeds for these two modes are given in the following sections.

Mode I Operation-Maximum Torque Curve

The general torque equation for electric machine is mentioned in Eqn. 3.33 as:

$$\tau_{mg-elec} = \psi_m I cos\gamma + 0.5(\xi - 1) L_d I^2 sin2\gamma \tag{3.42}$$

In Mode I operation, electric machine works at a constant torque corresponding to maximum torque per ampere current angle γ_m. The maximum torque per ampere current angle $\gamma_m$is calculated by differentiating equation 3.33 with respect to γ with $I = I_c$. If $\xi > 1$:

$$sin\gamma_m = \frac{-\psi_m + \sqrt{\psi_m^2 + 8(\xi-1)^2 L_d^2 I_c^2}}{4(\xi-1)L_d I_c} \tag{3.43}$$

and if $\xi = 1$, then $sin\gamma_m = 0$.

The rated torque $\tau_k$is obtained by substituting $\gamma = \gamma_m$and $I = I_c$into equation 3.33 to give:

$$\tau_{mg-elec} = \psi_m I_c cos\gamma_m + 0.5(\xi-1)L_d I_c^2 sin2\gamma_m \tag{3.44}$$

The base speed ω_b can be found by substituting $\gamma = \gamma_m$, $V = V_c$, $I = I_c$into equation 3.36.

Mode II Operation-Maximum Torque Curve

The rated current maintains in the motor as the speed increases, however the current angle increases from $\gamma_m$to larger values so as to maintain the rated voltage. For a given γ in mode II, maximum torque is given by substituting $V = V_c$, $I = I_c$into equations 3.33 as:

$$\tau_{max-mg-ele} = \psi_m I_c cos\gamma + 0.5(\xi-1)L_d I_c^2 sin2\gamma \tag{3.45}$$

where γ changes from γ_m calculated (Eqn. 3.43) to 90 degrees.

Note that the torque equations shown in section 3.3.1 had per phase values. The total torque τ_m of the electric machine can be obtained by:

$$\tau_m = pm_p T_m \tag{3.46}$$

where $m_p$is the number of phases of the electric machine and p is the number of pole pairs.

Electrical Power Model

In order to find the power at each given torque and speed, we need to calculate the corresponding current and current angle γ_m. We first find $\gamma$by solving Eqn. 3.36 for γ. Now that the current angle is found we can plug in its value along with the given torque to Eqn.3.33 and solve it for I. At this point both the current and current angle are calculated. The next step is to find the electrical power P_e by using:

$$P_e = m_p(V_d I_d + V_q I_q) \tag{3.47}$$

which is equal to:

$$P_e = m_p(-V_d I sin\gamma + V_q I cos\gamma) \tag{3.48}$$

where $m_p$is the number of phases of the electric machine and V_d and V_q can be calculated using Eqn.3.31 and Eqn.3.32 respectively.

The maximum output power generated by the model is shown in Fig. 3.9. The maximum torque curve and the efficiency plot can also be found on Fig. 3.8

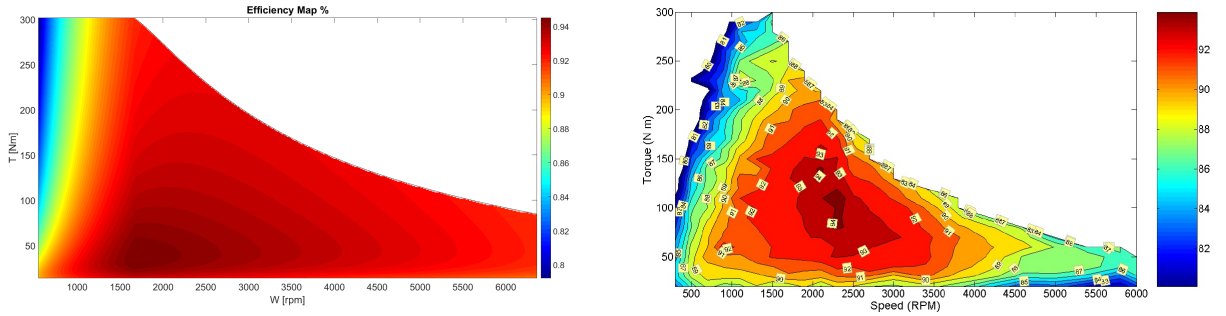

(a) Efficiency map generated by the toolkit

(b) Efficiency map generated from the experimental data of Toyota Prius 2004 [13]

Figure 3.8: Comparing the output results of the simulation toolkit with the experimental data of Toyota Prius 2004

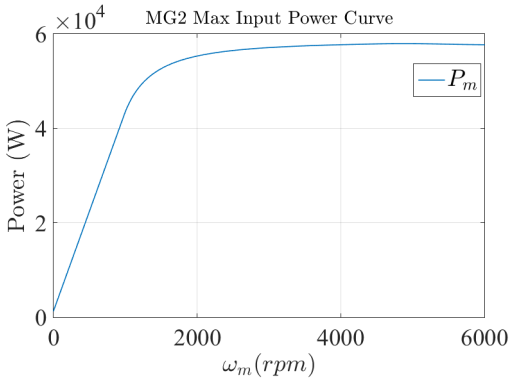

Figure 3.9: Power vs Rotational Speed (generated by the simulation toolkit)

3.3.2 IPMSM Inductance and Resistasnce Model

Designing a PM motor is a challenging and complicated process. This complexity rises from the large number of design variables, sensitivity of the model's performance to the topology, the involved and complicated equations, and nonlinearities. In this section an analytical model for an IPM synchronous motor is proposed based on the work done by Soong [49], which would be used later to optimize the design of the electric motor. First analytical methods of calculating the q-axis and d-axis inductance is reviewed. Then the method for calculating the L_d and L_q is discussed.

Winding Factors

The equations in this section are based on the work done by Miller [30].

The first step to calculate the inductances is to calculate the number of sine-distributed series turns per phase N_{sine}which can be found by:

$$N_{sine} = \frac{4}{\pi} k_{\omega 1} N_{ph} \tag{3.49}$$

$$N_{ph} = \frac{N_{coil} T_{co}}{m_p} \tag{3.50}$$

where $N_{ph}$is the number of series turns per phase, $N_{coil}$is the number of coils, $T_{co}$is the number of turns per coil and $k_{\omega 1}$is the fundamental winding factor which is given by:

$$k_{\omega 1} = k_{d1} k_{p1} k_{s1} \tag{3.51}$$

where k_{d1}, k_{p1}, and $k_{s1}$are the fundamental distribution factor, chord factor and skew factor of the winding respectively. Distribution factor is defined to take into account that the winding is not concentrated in a single slot, but is distributed over a number of slots. The fundamental distribution factor $k_{d1}$is defined by:

$$k_{d1} = \frac{sin(q\gamma_p/2)}{q sin(\gamma_p/2)} \tag{3.52}$$

where γ is the electrical slot pitch angle and q is number of slots per pole per phase. For a winding which is short-pitched by ϵ electrical degrees, the fundamental pitch factor is $k_{p1}$is:

$$k_{p1} = cos\frac{\epsilon}{2} \tag{3.53}$$

For reducing the torque ripple, skew is often used. In this model, it is assumed that there is no skew and as a result: $k_{s1} = 1$.

Effective Airgap

There are two effective airgaps defined in the literature: mechanical airgap (g_{mech}) and effective radial airgap (g'). The effective radial airgap is given by:

$$g' = g_{mech} k_{cr} k_{cs} \tag{3.54}$$

where k_{cr} and are rotor and stator Carter's coefficients respectively. The Carter's coefficient k_{cr} can be calculated by:

$$k_{cr} = \frac{w_t + w_s}{w_{t+(1-\sigma)w_s}} \tag{3.55}$$

where w_t and $w_s$are tooth width and slot opening width respectively. σ is a function of airgap and tooth width. For open slots Carter's coefficient is [49]:

$$\sigma_o = \frac{2}{\pi}[arctan\frac{w_s}{2g_{mech}} - \frac{g}{w_s}ln(1 + (\frac{w_s}{2g_{mech}})^2)] \tag{3.56}$$

If the slot is a semi-closed then the Carter's coefficient will be:

$$\sigma_{sc} = \sigma_o + 0.364(\frac{w_s}{g_{mech}})^{2/3} \tag{3.57}$$

Q and D Axis Magnetizing Inductance

The leakage inductance $L_1$is much smaller than the q-axis magnetizing inductance L_{qm}, hence the q-axis inductance is:

$$L_q = L_{qm} + L_1 \tag{3.58}$$

The magnetizing inductance L_m is given by [28]:

$$L_m = \frac{3\pi\mu_o N_{sine}^2 l r_1}{8p^2 g'} \tag{3.59}$$

where $N_{sine}$and g' can be calculated by 3.49 and 3.54, l, r_1,and p are the stack length, airgap radius and number of pole pairs respectively. Here, we have a radially laminated motor. As a result, $L_m$and $L_{qm}$are equal to each other.

If a number of lamination layers inserted inside of the satator in a way that the flux lines are always perpendicular to the layers, the field distribution wouldn't change [29]. However, it would increase the inductance which is termed as intrinsic magnetizing d-axis inductance L_{dm}:

$$L_{dm} = \frac{3\pi\mu_0 N_{sine}^2 l}{8pa} \tag{3.60}$$

where a is the rotor insulation ratio.

Slot-Leakage Inductance

The slot leakage per phase L_{slt} is:

$$L_{slt} = \frac{4N_{ph}^2 m_p \mu_0 l}{N_{slot}} P_s \tag{3.61}$$

where m_p and N_{slot} are number of stator phases and number of stator slots respectively and $P_s$is the total slot permeance ratio which is the sum of the slot permeances for each of the three sections shown in figure3.10

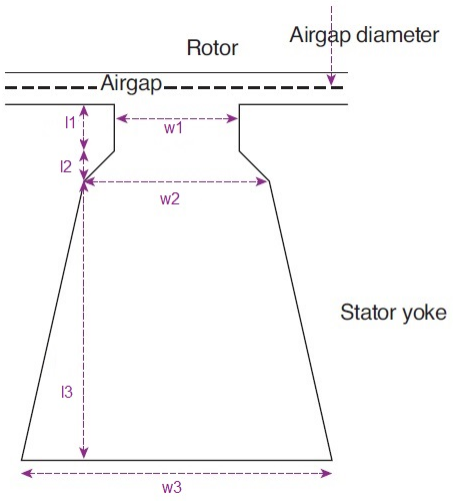

Figure 3.10: Trapezoidal slot dimensions [8]

The permeance of the slot section closest to the airgap neglecting fringing is:

$$P_{s1} = \frac{l1}{w1} \tag{3.62}$$

If $l_1 \ll w_1$then we should take into account the fringing into airgap and P_{s1}can be found by:

$$P_{s1} = \frac{l1}{w1} + \frac{1}{\pi} ln \frac{r_b}{r_a} \tag{3.63}$$

where $r_a$and $r_b$are half the slot opening and slot pitch minus r_a. The permeance ratio P_{s2} and of the tange's inside are given by:

$$P_{s2} = \frac{l_2}{w_2 - w_1} ln \frac{w_2}{w_1} \tag{3.64}$$

The permeance ratio P_{s3} of the main body for trapezoidal slots is given by:

$$P_{s3} = \frac{l_3}{w_3} \frac{4\beta^2 - \beta^4 - 4ln\beta - 3}{4(1-\beta)(1-\beta^2)^2} \tag{3.65}$$

where:

$$\beta = \frac{w_2}{w_3} \tag{3.66}$$

Moreover, the slot geometry parameters mentioned above can be calculated as:

$$l_1 = r_a \tag{3.67}$$

$$l_2 = (R_1 + r_1)tan(\frac{\pi}{N_{slot}}) - r_1 - w_{tb} \tag{3.68}$$

$$l_3 = SlotD - l_1 - l_2 \tag{3.69}$$

$$w_1 = 2r_a \tag{3.70}$$

$$w_2 = 2(R_1 + l_1 + l_2)tan(\frac{\pi}{N_{slot}}) - w_{tb} \tag{3.71}$$

$$w_3 = 2(R_1 + SlotD)tan(\frac{\pi}{N_{slot}}) - w_{tb} \tag{3.72}$$

where w_{tb} is the tooth width at base,$R_1$and r_1 are stator inner radius and rotor radius respectively.

End-Winding Leakage Inductance

Calculating the end-winding inductance is a complicated process and usually done by finite element analysis. Here a very simple method developed by [2] for calculating of the inductance is given, which is not based on the FEM analysis :

$$L_{OneTurn} = \mu_0 \frac{D_{end}}{2}((1 + \frac{R_w^2 D_{end}^2}{2})ln(\frac{4D_{end}}{R_w}) + (\frac{R_w}{D_{end}})^2 \frac{1}{6} - 1.75) \tag{3.73}$$

$$L_{End} = L_{OneTurn} p N_{end}^2 X_{end} \tag{3.74}$$

where X_{end} is the end-turn leakage adjustment factor.

Total d and q Inductances

Finally the d-axis inductance L_d and L_q are given by:

$$L_d = L_{dm} + L_{End} + L_{slt} \tag{3.75}$$

$$L_q = L_{qm} + L_{End} + L_{slt} \tag{3.76}$$

Stator Resistance and copper loss

For finding the copper loss, stator resistance is needed. The first step is finding the mean length per turn. The mean length per turn (MLT_{stack}) is composed of the straight (useful) section in the stator and the useless section in the end-winding (MLT_{end}).

$$MLT = MLT_{end} + MLT_{stack} \tag{3.77}$$

$$MLT_{stack} = 2l \tag{3.78}$$

$$MLT_{end} = \pi D_{end} \tag{3.79}$$

where D_{end} is the mean diameter of the end-winding and is given by:

$$D_{end} = \frac{m_p q}{N_{slot}}(2R_1 + SlotD) \tag{3.80}$$

where N_{slot} is the number of slots, R_1 is the stator inner radius, and $SlotD$ is the slot depth measured from the airgap. The phase resistance is given by:

$$R_{ph} = \frac{\rho_{cu} L_{con}}{A_{cu}} \tag{3.81}$$

where ρ_{cu} is the copper resistivity, L_{con} is the total length of the conductors, and A_{cu} is the cross sectional area of the copper. $L_{con}$and $A_{cu}$are given by:

$$l_{con} = \frac{N_{coil} T_{co} MLT}{m_p} \tag{3.82}$$

$$A_{cu} = \pi NSH \frac{W_d^2}{4}$$

where $N_{coil}$is the number of coils, $T_{co}$is the number of turns per coil,NSH is the number of strands per phase, and W_d is the bare copper wire diameter.

3.3.3 Electric Machine Inertia Model

The electric machine mass is comprised of the mass of stator core M_{sc} , stator teeth M_{st}, rotor core M_{rc}, permanent magnet M_{pm}, and stator winding M_{sw}. Analytical equations to find each of these quantities are based on work by Duan [14] and modified as appropriate for IPMSM architecture using data from Oak Ridge National Laboratory [13]. First, the stator core mass is given by

$$M_{sc} = \frac{\pi}{4}\rho_s (D_{so}^2 - (D_{si} + 2SlotD)^2) l \tag{3.83}$$

Stator tooth mass is given by:

$$M_{st} = N_{slot*}\rho_s * SlotD * w_{tb} * l \tag{3.84}$$

Rotor core mass can be calculated as:

$$M_{rc} = \rho_s l(\frac{\pi}{4}((2r_o)^2 - D_{ri}^2) - N_{PM}w_m h_m) \tag{3.85}$$

where $r_o$is rotor outer diameter radius and considered as:

$$r_o = \frac{D_{si}}{2} - g_{mech} \tag{3.86}$$

Mass of the permanent magnet is given by:

$$M_{pm} = N_{PM}\rho_{pm} l_m h_m w_m \tag{3.87}$$

Finally, the stator winding mass can be calculated by:

$$M_{sw} = 3\rho_{cu} A_{cu} l_{con} \tag{3.88}$$

where $D_{so}$is the stator outer diameter, D_{ri} is the rotor inner diameter, D_{si} is the stator inner diameter, l is the stack length, $h_m$is the magnet thickness, l_m is the magnet length, w_m is the magnet width, N_{pm} is the number of magnets, ρ_s, ρ_{cu}, and $\rho_{pm}$are the mass densities of steel, copper, and the permanent magnets respectively. In the end the total mass M_{motor} of the electric motor is:

$$M_{motor} = M_{sc} + M_{st} + M_{rc} + M_{pm} + M_{sw} \tag{3.89}$$

The moment of inertia of the rotor J_{rotor} assuming it to be a uniform cylinder of density equal to that of iron is given by

$$J_{rotor} = 0.5(m_{rc} + m_{pm})0.25(D_{ri}^2 + (2r_o)^2 + 0.5\rho_s(\frac{\pi}{4}D_{ri}^2 l)\frac{D_{ri}^2}{4} \tag{3.90}$$

The design parameters which are used in the models are listed in Table 3.3 and 3.4. The values in Table 3.3 and 3.4are adopted from Toyota Prius 2004 [8, 12, 13]. The geometry related parameters are scaled with respect to the design vatiables of the models as the design variables change in the process of design optimization.

Table 3.3: Design parameters used in the motor model based on the values of Toyota Prius 2004

Design Parameter	Value	Design Parameter	Value
Number of pole pairs (p)	8	Rated Voltage (V_c)	500 (V)
Number of phases (m_p)	3	# of slots per pole per phase (q)	2
Stator tooth depth (l_1)	0.762 (mm)	Winding chording angle(ϵ)	0
Stator slot opening ($2r_a$)	1.93 (mm)	fundamental skew factor (k_{s1})	1
Stator outer diameter (D_{so})	346 (mm)	mechanical airgap (g_{mech})	0.73 (mm)
Number of coils (N_{coil})	24	rotor insulation ratio	0.1
Number of turns per coil (T_{co})	9	# of strands per phase (NSH)	2
airgap size (g')	1.38 (mm)	slot depth ($SlotD$)	33.5 (mm)
Slot opening width (w_s)	3.9 (mm)	tooth width at base (w_{tb})	8.185 (mm)
Mass density of steel (ρ_s)	7800 ($\frac{kg}{m^3}$)	magnet thickness (h_m)	6.5 (mm)
Copper resistivity (ρ_{cu})	$1724 * 10^{-11}(\frac{\Omega}{m})$	magnet length (l_m)	83.1 (mm)
Bare copper, wire diameter	0.91 (mm)	magnet width (w_m)	18.9 (mm)
End leakage adjustment factor (X_{end})	0.5	Mass density of the magnet (ρ_{pm})	7550 ($\frac{kg}{m^3}$)

Table 3.4: Design parameters used in the generator model based on the values of Toyota Prius 2004

Design Parameter	Value	Design Parameter	Value
Number of pole pairs (p)	4	Rated Voltage (V_c)	500 (V)
Number of phases (m_p)	3	# of slots per pole per phase (q)	2
Stator tooth depth (l_1)	0.762 (mm)	Winding chording angle(ϵ)	0
Stator slot opening ($2r_a$)	1.70 (mm)	fundamental skew factor (k_{s1})	1
Stator outer diameter (D_{so})	236.2 (mm)	mechanical airgap (g_{mech})	0.64 (mm)
Number of coils (N_{coil})	24	rotor insulation ratio	0.1
Number of turns per coil (T_{co})	9	# of strands per phase (NSH)	2
airgap size (g')	0.695(mm)	slot depth ($SlotD$)	29.51 (mm)
Slot opening width (w_s)	3.9 (mm)	tooth width at base (w_{tb})	7.209 (mm)
Mass density of steel (ρ_s)	7800 ($\frac{kg}{m^3}$)	magnet thickness (h_m)	5.72 (mm)
Copper resistivity (ρ_{cu})	$1724 * 10^{-11}(\frac{\Omega}{m})$	magnet length (l_m)	29.85 (mm)
Bare copper, wire diameter	0.91 (mm)	magnet width (w_m)	16.64(mm)
End leakage adjustment factor (X_{end})	0.5	Mass density of the magnet (ρ_{pm})	7550 ($\frac{kg}{m^3}$)

3.4 Battery

The battery is one of the most critical components in PHEV powertrain design. Many electrochemical models have been developed to represent the battery performance [36, 52, 54], including those by Mierlo et al. [52]. In this thesis, we use the model by Mierlo et al. to represent a lithium-ion battery pack for a PHEV.

3.4.1 Battery State of Charge Model

The equivalent circuit of the battery model is shown in Fig. 3.11.

As we have described the battery is an equivalent circuit model, the equations describing its current flow (I_b) and

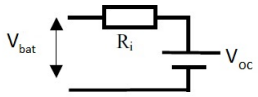

Figure 3.11: Equivalent scheme of a simple battery model.

rate of change of SOC are given as:

$$I_b = \frac{V_{oc} - \sqrt{V_{oc}^2(SOC) - 4P_{batt}R_i(SOC)}}{2R_i(SOC)} \tag{3.91}$$

$$\frac{dSOC}{dt} = -\frac{I_b}{Q} \tag{3.92}$$

where SOC is the state of the charge of the battery, $V_{oc}(SOC)$is the open circuit voltage as a function of SOC, $R_i(SOC)$is the internal resistance as a function of SOC, and Q is the capacity of the battery. If we connect N_s series cells and N_p parallel cells together, then the open circuit voltage, internal resistance, and the capacity of the whole battery package can be given by:

$$V_{oc}(SOC) = N_s V_{oc,cell}(SOC) \tag{3.93}$$

$$R_i(SOC) = \frac{N_s}{N_p} R_{i,cell}(SOC) \tag{3.94}$$

$$Q = N_p Q_{cell} \tag{3.95}$$

P_{batt}can be calculated as:

$$P_{batt} = P_{MG1} + P_{MG2} \tag{3.96}$$

where $P_{MG1}$and P_{MG2} are the power demand of generator and motor respectively.

Considering the battery dynamics, both the $V_{oc}$and $R_i$are functions of SOC. For a given battery cell topology the battery open circuit voltage and internal resistance curves for one cell are shown in figure 3.12.

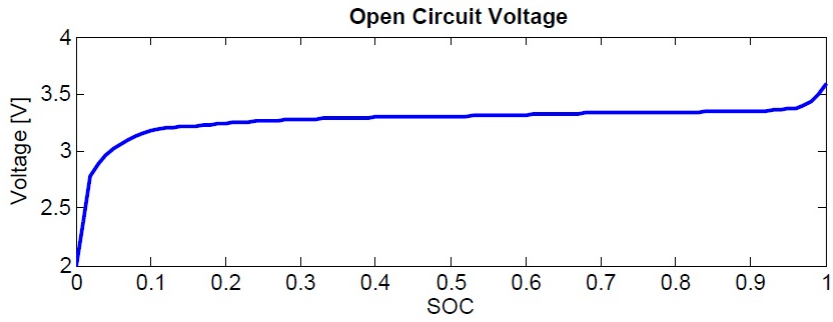

(a) Open circuit voltage

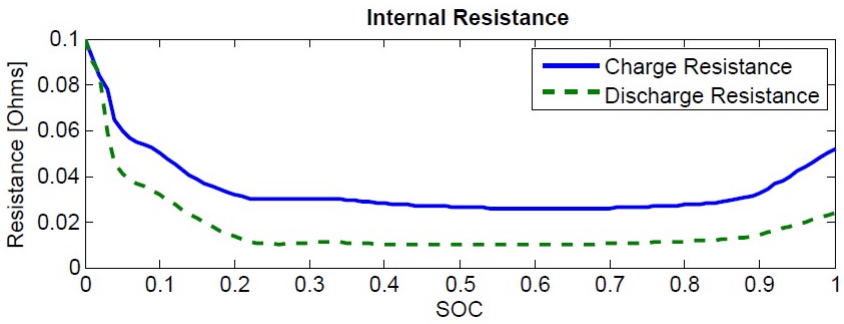

(b) internal resistance

Figure 3.12: Equivalent circuit battery model identified from commercial lithium-ion cells with LiFePO4 cathode [31] (Battery model: A123 Systems ANR26650M1A) a) Open circuit voltage b) internal resistance.

3.4.2 Battery Inertia Model

The battery pack mass is calculated assuming that the mass of each cell is known. In this respect, the total mass would be the product of total number of cells and the mass of each individual cell:

$$m_{batt} = N_s N_b m_{cell} \tag{3.97}$$

where m_{cell} is the mass of each individual battery cell. The parameters used in the battery model are listed in Table. 3.5.

Table 3.5: Battery design parameters (Battery model: A123 Systems ANR26650M1A)

Design Parameter	Value
mass of each cell (m_{cell})	0.0727 (kg)
battery capacity (Q)	2.3 (Ah)

Based on the model discussed in this section, a Matlab code is written which gets two design variables N_s, $N_p$and calculates the $\dot{SOC}$, battery pack mass, and output current as a function of SOC.

Chapter 4: MDSDO OF PHEV POWERTRAINS

Two studies have been considered in this thesis:

1. Component sizing of the battery along with the supervisory control of the engine, motor, and generator to minimize the operating cost of the PHEV (energy cost).

2. Component sizing of the entire propulsion system (engine, motor, generator, battery, and transmission) along with the supervisory control of the engine, motor, and generator to minimize the operating cost of the PHEV (energy cost).

The aim of these two studies is comparing the effect of optimizing the control trajectory of the system and only considering the battery's design as an unknown, versus optimizing the design and control of the whole propulsion system of the PHEV on the operating cost. A similar study has been done before by Edgart et al. [15]. The main differences between this thesis and their research are as follows:

1. They use scaling factors exclusively to represent the component design variables, and these variables are merely dimensionless power ratings that scale the size of their performance curves for different designs. Although some of our performance curves (engine and battery) are effectively scaled for different designs, we still use physically meaningful design variables to represent each of those components. Moreover, the motor/generator models used in this thesis do not scale their performance curves for different designs but rather compute distinct performance curves based on different values of physically meaningful design variables.

2. Their formulations require all of their functions (objectives and constraints) to be convex. However, there is no such restriction in our approach.

3. Their models are less complex in terms of the number of variables and functional representation.

4. By using a commercially available software known as GPOPS-II, we were able to use a more efficient discretization approach (hp-adaptive gaussian quadrature collocation, LGR collocation method) than their approach, which simply uses equally-spaced discretized points.

In the next sections, an overview of the two different optimization approaches is discussed.

The objective function used in this study is:

$$\min_{d,x(t),u(t),t} \Phi = \int_{t_0}^{t_f} (C_{fuel}\dot{m}_{fuel}(d, x(t), u(t), t) + C_{elec}P_{batt}(d, x(t), u(t), t))dt \tag{4.1}$$

where C_{fuel} and $C_{elec}$are the cost of fuel and electricity respectively. Moreover, $x(t)$ and $u(t)$ are state decision variable vector and control input vector respectively. Finally, d is the design variable vector.

Table 4.1: Energy Costs

Parameter	Value
electricity cost (C_{elec})	0.13 ($\$/kWh$)
fuel cost (C_{fuel})	2.76 ($\$/gallon$)

4.1 Battery Design & PHEV Supervisory Control

The first part of the optimization is done based on the assumption that the design variables of the motor, generator, engine and final drive ratio are fixed and only the battery design variables can change. The objective and constraints of this problem are as follows:

$$\min_{d,x(t),u(t),t} \Phi_{batt} = \min_{d,x(t),u(t),t} \int_{t_0}^{t_f} (C_{fuel}\dot{m}_{fuel}(d,x(t),u(t),t) + C_{elec}P_{batt}(d,x(t),u(t),t))dt \tag{4.2}$$

subject to path constraints:

$$\omega_{e,min}(d) \leq \omega_e \leq \omega_{e,max}(d) \tag{4.3}$$

$$\omega_{m,min}(d) \leq \omega_m \leq \omega_{m,max}(d) \tag{4.4}$$

$$\omega_{g,min}(d) \leq \omega_g \leq \omega_{g,max}(d) \tag{4.5}$$

$$SOC_{min} \leq SOC \leq SOC_{max} \tag{4.6}$$

$$\tau_{e,min}(d,x(t)) \leq \tau_e \leq \tau_{e,max}(d,x(t)) \tag{4.7}$$

$$\tau_{g,min}(d,x(t)) \leq \tau_g \leq \tau_{g,max}(d,x(t)) \tag{4.8}$$

$$\tau_{m,min}(d,x(t)) \leq \tau_m \leq \tau_{m,max}(d,x(t)) \tag{4.9}$$

$$-\frac{V_{oc}^2(d)}{4R_i(d)} \leq P_{batt}(x(t),u(t)) \leq \frac{V_{oc}^2(d)}{4R_i(d)} \tag{4.10}$$

$$V_{veh,min} \leq \frac{\omega_m r_{tire}}{K} \leq V_{veh,max} \tag{4.11}$$

$$\tau_g\omega_g < 0 \tag{4.12}$$

$$|\tau_g\omega_g| - |\tau_e\omega_e| \leq 0 \tag{4.13}$$

$$\dot{\omega}_{e,min} < \dot{\omega}_e < \dot{\omega}_{e,max} \tag{4.14}$$

design variable constraints:

$$N_{s,min} \leq N_s \leq N_{s,max} \tag{4.15}$$

$$N_{p,min} \leq N_p \leq N_{p,max} \tag{4.16}$$

where t is time, and vectors d,$x(t)$, and $u(t)$ are defined as follow:

$$d = [N_s, N_p] \tag{4.17}$$

$$x(t) = [\omega_e(t), \omega_m(t), SOC(t)] \tag{4.18}$$

$$u(t) = [\tau_e(t), \tau_g(t), \tau_m(t)] \tag{4.19}$$

As discussed in the earlier chapters, the aim of this study is to solve the co-design problem using direct transcription method. Direct transcription transforms infinite dimensional control design problems into finite dimensional nonlinear programming problems [3] [22]. In order to solve the problem, GPOPS-II [39],a DT based MATLAB software for solving multiple-phase optimal control problems was implemented. GPOPS-II uses an hp-adaptive version of the Legendre-Gauss-Radau (LGR) orthogonal collocation method [17, 39]. After discretizing the problem, GPOPS-II sends the values of the collocation points to an interior point optimization toolbox called IPOPT [53]. IPOPT uses a primal-dual interior point algorithm with a filter line search for non-linear programming. The NLP problem then would be solved using IPOPT, and the final optimal state and control trajectories as well as time independent variables will be output of the GPOPS-II. The settings used in GPOPS-II are listed in Table. 4.2.

Table 4.2: GPOPS/IPOPT settings

Field	Value
NLP solver	IPOPT
Linear solver	ma57
ipopt tolerance	10^{-6}
ipopt max iteration number	3000
derivative supplier	sparseCD
derivative level	second
scale method	automatic bounds
mesh method	hp-LiuRao-Legendre
mesh tolerance	10^{-3}
mesh maximum iteration	45
minimum collocation points in a mesh	2
maximum collocation points in a mesh	14

In this study, the vehicle should follow a predefined drive schedule trajectory. The chosen road profile in this study

is US06 which is shown in Fig.4.1. Given the vehicle's speed (V_{veh}) and by using Eqn. 4.20 we can find ω_m, and then we set the upper and lower bound on this state ($\pm 5km/h$).

$$\omega_m = \frac{KV_{veh}}{r_{tire}} \tag{4.20}$$

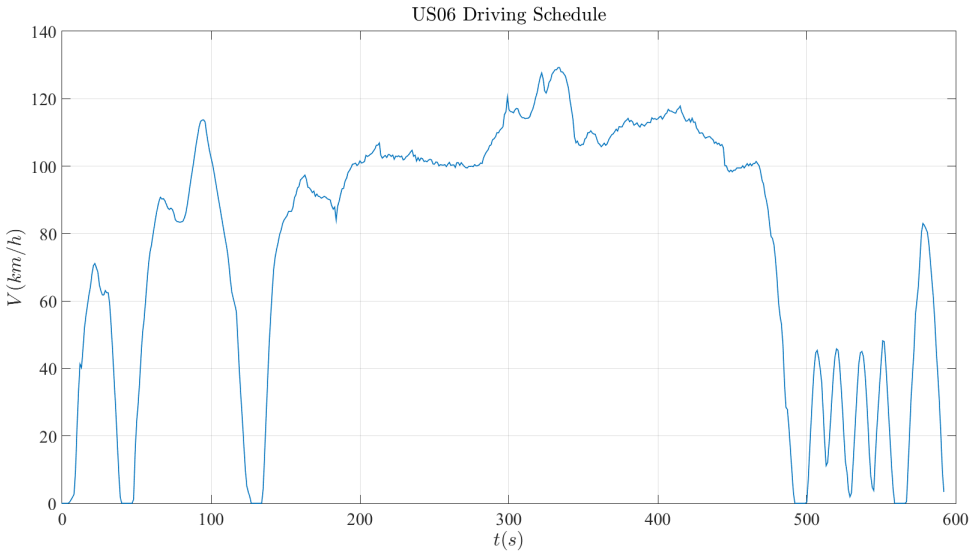

Figure 4.1: US06 drive schedule

The aforementioned problem is solved using GPOPS-II [39]. The optimal value of the objective function, as well as the optimal value for the design variables in this study are shown in Table.4.3. The run-time of the algorithm was about 27 hours using a computer with 16 GB of ram and CPU model: Intel(R) Xeon(R) CPU E5-2637 v3 @ 3.50 GHZ 3.5 GHZ (2 processors)

Table 4.3: Optimal values for battery design problem

Variable	Optimal Value
objective function (fuel and electricity cost)	$ 0.1841
number of series cells in the battery pack (N_s)	122.55
number of series cells in the battery pack (N_p)	141.2

The optimal trajectories of control inputs and states are shown in Fig. 4.2 and Fig. 4.3 respectively.

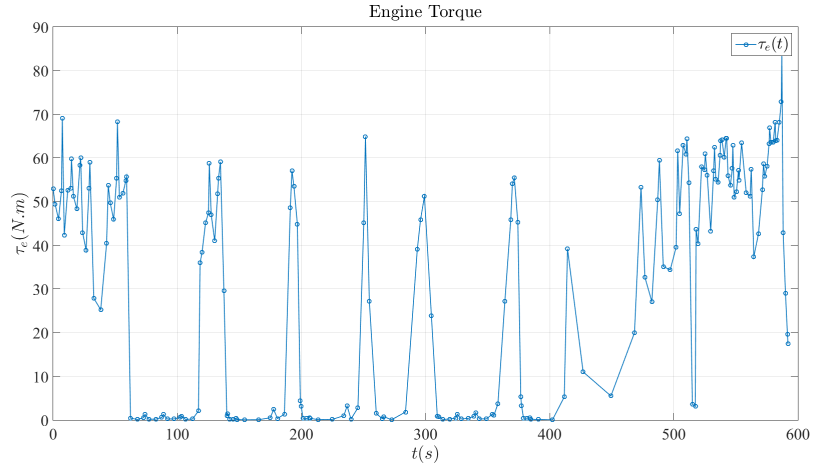

(a) Engine Torque (τ_e)

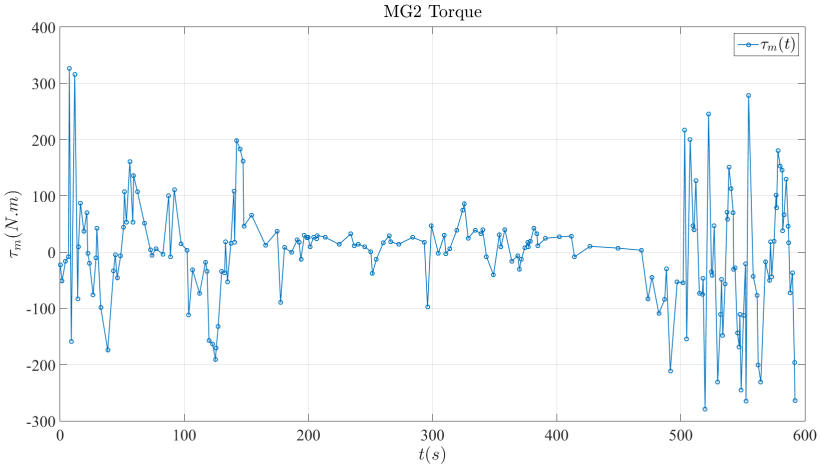

(b) Motor Torque (τ_m)

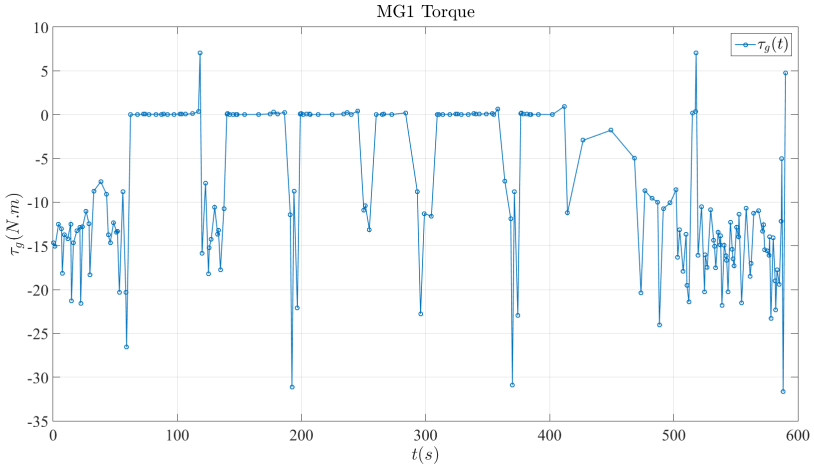

(c) Generator Torque (τ_g)

Figure 4.2: Optimal control input trajectories for battery study

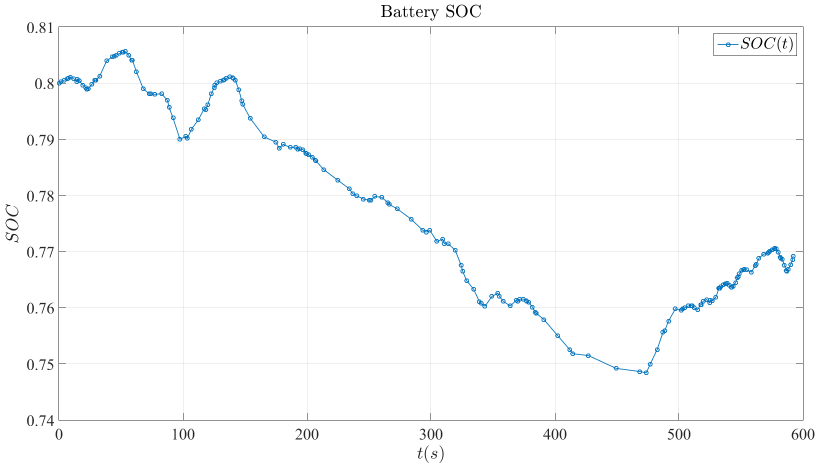

(a) SOC

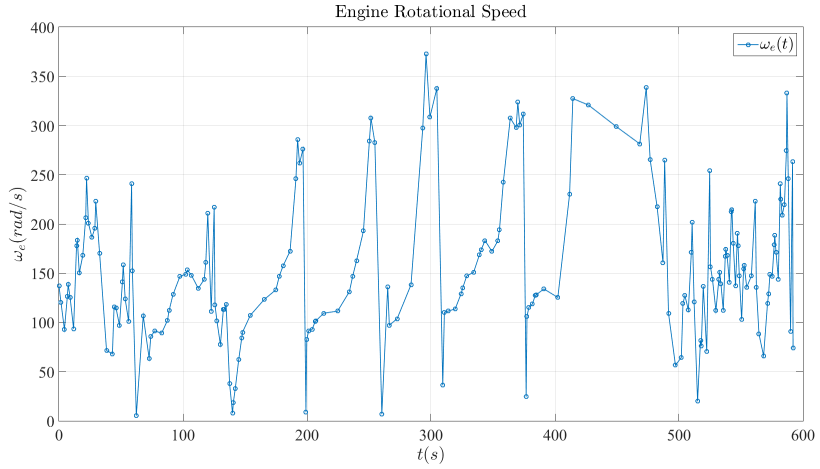

(b) Engine rotational speed (ω_e)

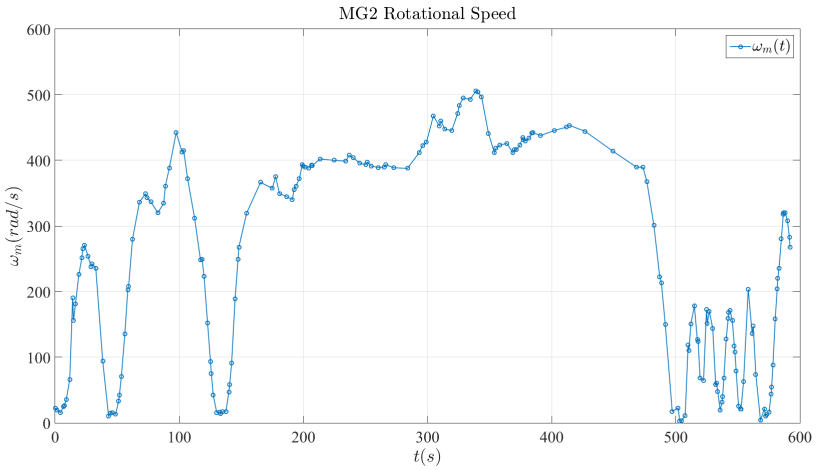

(c) Motor rotational speed (ω_m)

Figure 4.3: Optimal trajectories of states for battery sudy

As a sense check of the results we have calculated the total power demand for satisfying the US06 drive schedule and then compared it with the total tractive power of engine and motor. The power demand at the wheels can be calculated as:

$$P_{demand} = \tau_{demand}\omega_m \tag{4.21}$$

Where P_{demand} is the power demand at the wheels and τ_{demand} is the demanded torque at the wheels and can be calculated using equations: 4.20,3.7,3.9 . The total generated power of engine and motor, using the values of the optimization study, can be calculated study as follow:

$$P_{tractive} = \tau_e\omega_e + \tau_m\omega_m \tag{4.22}$$

This comparison is illustrated in Fig.4.4.

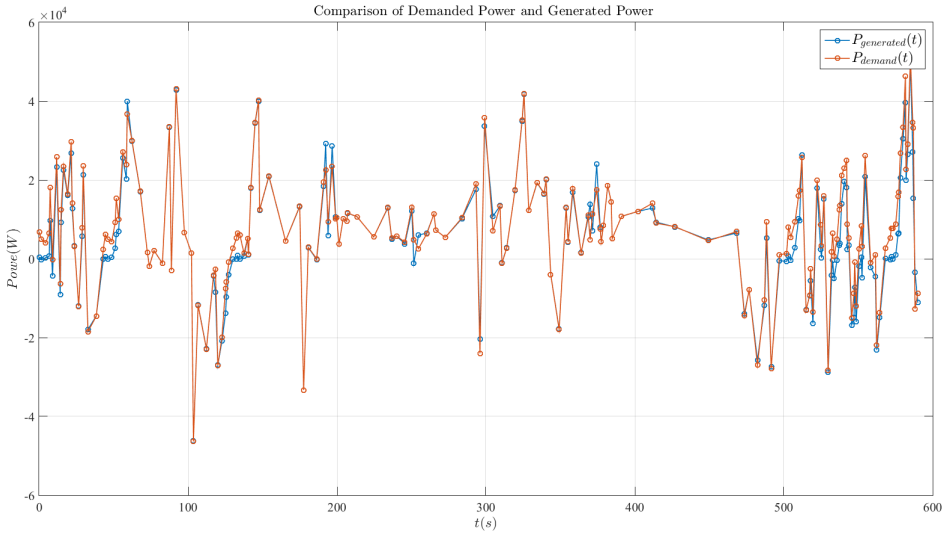

Figure 4.4: Comparison of demanded power and generated tractive power for the battery study

4.2 Powertrain Design and PHEV Supervisory Control

This part of the optimization is performed based on the assumption that the design of the engine, battery, motor, generator, and final drive ratio are unknown and needed to be found via the optimization. In this thesis, each component is designed analytically through the corresponding design variables associated with them and the performance of them are calculated based on those designs. The objective function would be the same as the objective function in section 4.1, but with a different d vector:

$$\min_{d,x(t),u(t),t} \Phi_{PT} = \min_{d,x(t),u(t),t} \int_{t_0}^{t_f} (C_{fuel}\dot{m}_{fuel}(d,x(t),u(t),t) + C_{elec}P_{batt}(d,x(t),u(t),t))dt \tag{4.23}$$

subject to path constraints:

$$\omega_{e,min}(d) \leq \omega_e \leq \omega_{e,max}(d) \tag{4.24}$$

$$\omega_{m,min}(d) \leq \omega_m \leq \omega_{m,max}(d) \tag{4.25}$$

$$\omega_{g,min}(d) \leq \omega_g \leq \omega_{g,max}(d) \tag{4.26}$$

$$SOC_{min} \leq SOC \leq SOC_{max} \tag{4.27}$$

$$\tau_{e,min}(d,x(t)) \leq \tau_e \leq \tau_{e,max}(d,x(t)) \tag{4.28}$$

$$\tau_{g,min}(d,x(t)) \leq \tau_g \leq \tau_{g,max}(d,x(t)) \tag{4.29}$$

$$\tau_{m,min}(d,x(t)) \leq \tau_m \leq \tau_{m,max}(d,x(t)) \tag{4.30}$$

$$-\frac{V_{oc}^2(d)}{4R_i(d)} \leq P_{batt}(x(t),u(t)) \leq \frac{V_{oc}^2(d)}{4R_i(d)} \tag{4.31}$$

$$V_{veh,min} \leq \frac{\omega_m r_{tire}}{K} \leq V_{veh,max} \tag{4.32}$$

$$\tau_g \omega_g < 0 \tag{4.33}$$

$$|\tau_g \omega_g| - |\tau_e \omega_e| \leq 0 \tag{4.34}$$

$$\dot{\omega}_{e,min} < \dot{\omega}_e < \dot{\omega}_{e,max} \tag{4.35}$$

The design variable constraints are:

$$CR_{min} \leq CR \leq CR_{max} \tag{4.36}$$

$$D_{b,min} \leq D_b \leq D_{b,max} \tag{4.37}$$

$$L_{st,min} \leq L_{st} \leq L_{st,max} \tag{4.38}$$

$$R_{m,min} \leq R_m \leq R_{m,max} \tag{4.39}$$

$$l_{m,min} \leq l_m \leq l_{m,max} \tag{4.40}$$

$$I_{max,lower} \leq I_{max,m} \leq L_{max,upper} \tag{4.41}$$

$$R_{g,min} \leq R_g \leq R_{g,max} \tag{4.42}$$

$$l_{g,min} \leq l_g \leq l_{g,max} \tag{4.43}$$

$$I_{max,g,lower} \leq I_{max,g} \leq L_{max,g,upper} \tag{4.44}$$

$$N_{s,min} \leq N_s \leq N_{s,max} \tag{4.45}$$

$$N_{p,min} \leq N_p \leq N_{p,max} \tag{4.46}$$

where t is time, and vectors d,$x(t)$, and $u(t)$ are defined as follows:

$$d = [N_s, N_p, CR, D_b, L_{st}, R_m, l_m, I_{max,m}, R_g, l_g, I_{max,g}, K] \tag{4.47}$$

$$x(t) = [\omega_e(t), \omega_m(t), SOC(t)] \tag{4.48}$$

$$u(t) = [\tau_e(t), \tau_g(t), \tau_m(t)] \tag{4.49}$$

The options used in GPOPS-II are the same as the options mentioned in section 4.1 and are listed in Table.4.2. Constraints used in this study are the same as the constraint mentioned in section 4.1, however the design vector is different. The optimal results of this study along with the values from the study of section 4.1 are listed in Table 4.4. The run-time of the algorithm was about 35 hours using a computer with 16 GB of ram and CPU model: Intel(R) Xeon(R) CPU E5-2637 v3 @ 3.50 GHZ 3.5 GHZ (2 processors)

Design Parameters and Variables	Battery Only Optimization	System Level Optimization
N_s: number of seris cells in the battery pack	122.55	117.67
N_p: number of parallel cells in the battery pack	14.1	13.43
R_g: MG1 stator inner diameter	142.6 (mm)	140 (mm)
l_g: MG1 stack length	30.5 (mm)	30 (mm)
$I_{max,g}$: MG1 maximum current	75 (A)	75 (A)
R_m: MG2 stator inner diameter	161.9 (mm)	160 (mm)
l_m: MG2 stack length	84 (mm)	84 (mm)
$I_{max,m}$: MG2 maximum current	122.5 (A)	121.5 (A)
K: Final drive ratio	4.113	3.041
CR: Engine compression ratio	13	13
D_b:Engine piston bore diameter	75.52 (mm)	63 (mm)
L_{st}: Engine stroke length	84.7 (mm)	68 (mm)
objective function (fuel and electricity cost)	$ 0.1841	$ 0.1519

Table 4.4: Comparison between the results of the system level optimization and the battery only optimization

The optimal trajectories of control inputs and states are shown in Fig 4.5 and 4.6 respectively.

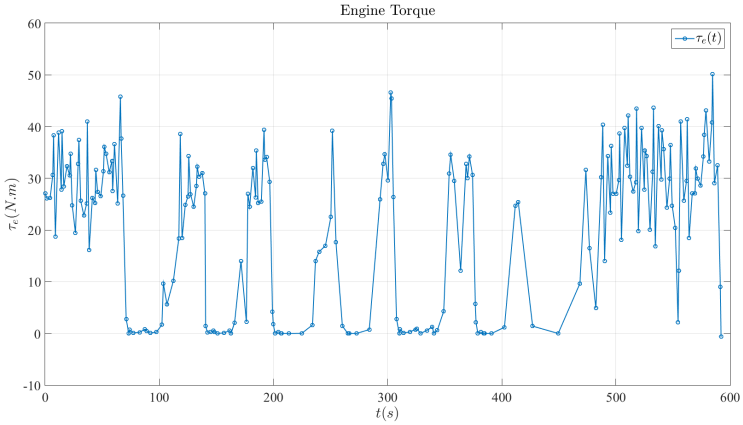

(a) Engine Torque (τ_e)

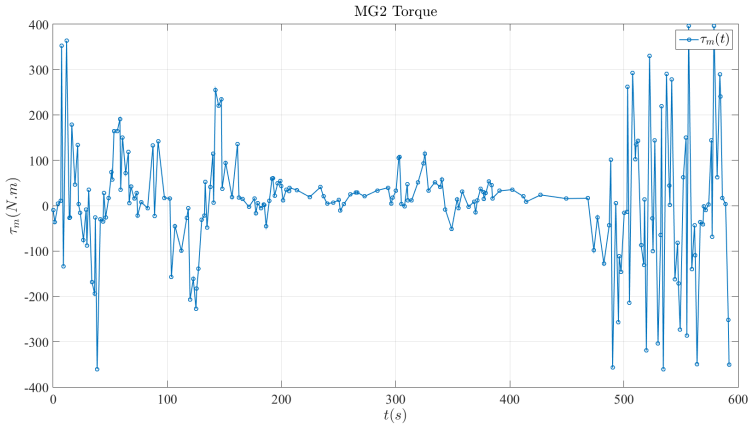

(b) Motor Torque (τ_m)

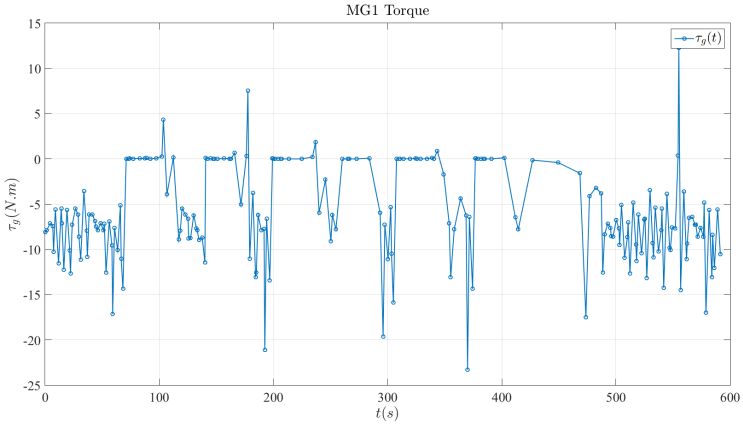

(c) Generator Torque (τ_g)

Figure 4.5: Optimal control input trajectories for powertrain study

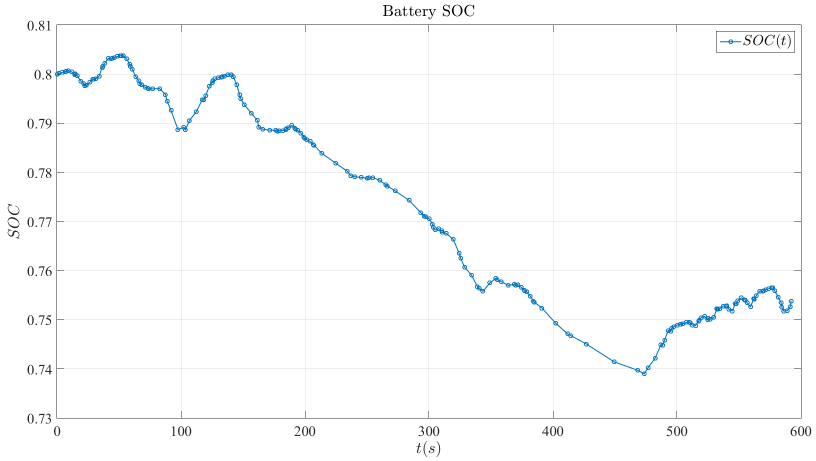

(a) SOC

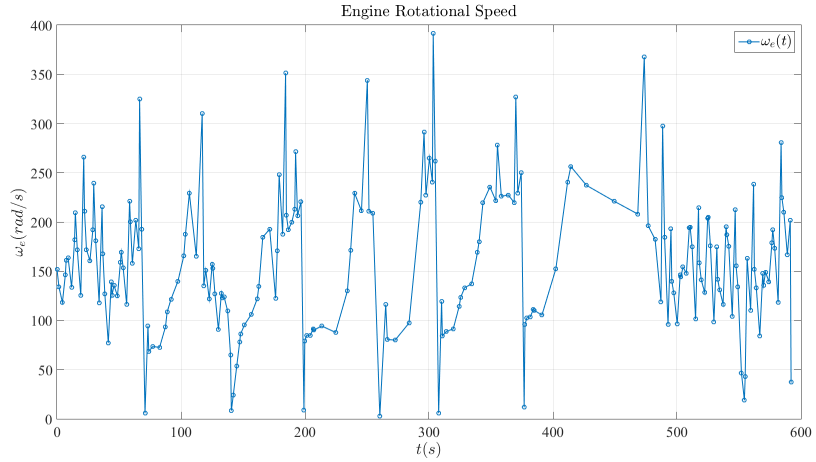

(b) Engine rotational speed (ω_e)

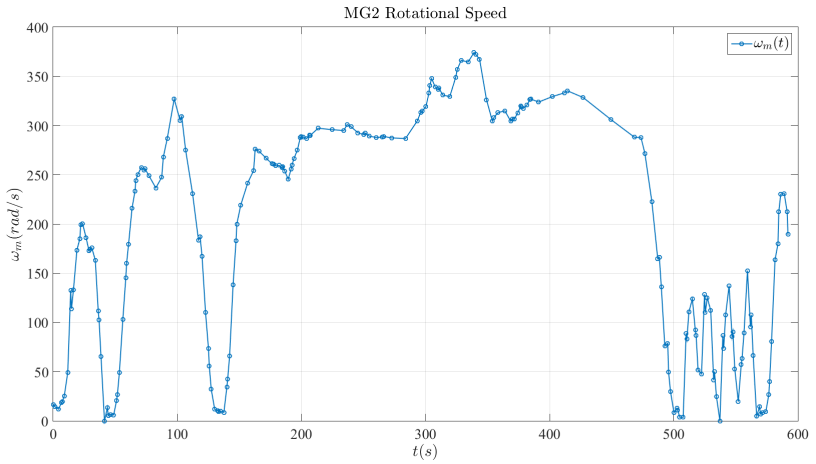

(c) Motor rotational speed (ω_m)

Figure 4.6: Optimal trajectories of states for powertrain study

Finally, the comparison between the generated tractive power and demanded power is shown in Fig.

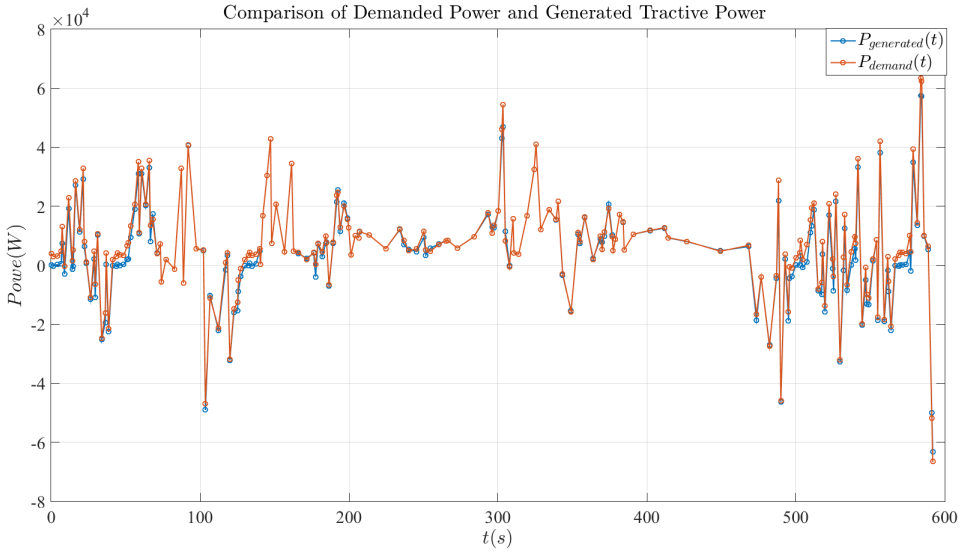

Figure 4.7: Comparison of demanded power and generated tractive power for the powertrain study

Chapter 5: CONCLUSION AND FUTURE WORK

The DT-based simultaneous problem formulation was extended successfully to a large-scale system design application, namely the co-design of PHEV powertrain. Two MDSDO studies for a power-split PHEV was performed in this thesis. The first study investigated the component sizing of the high-voltage battery along with the supervisory control of its engine, electric motor and generator such that the total system energy cost is minimized while satisfying the system performance-related constraints. The second study, investigated the component sizing of the complete powertrain, which includes the engine, electric motor, generator, transmission, and high-voltage battery, along with the supervisory control of the engine, electric motor, and generator for the same system decision objectives and constraints. In both these studies, detailed models were used which were capable of capturing the effect of meaningful design variables on the performance of the components. GPOPS-II [39], a commercially available software, was used to solve the optimization study using DT. By comparing the results of the two studies, it was shown that the objective function has decreased about 17.5% when the whole powertrain design was subjected to the optimization. This fact suggests that although sizing of the high voltage battery is an important factor, the co-design of the whole powertrain, can indeed reduce the operating cost of the vehicle even more.

An attempt was made to use fairly meaningful models in this thesis. A sophisticated model was developed for sizing the electric machine. The models that were used for the battery and engine also contained meaningful design variables; however to some extent, they were effectively scaling the performance curves for different designs. In this respect as a future work, we can use more detailed analytical models for engine and battery to study the effect of the co-design of the powertrain on the overall performance of the vehicle. Moreover, it was shown that DT can be used in large scale MDSDO studies. As a result we can implement the same approach to different large-scale systems.

Appendix A: DESIGN OPTIMIZATION, OPTIMAL CONTROL AND DIRECT TRANSCRIPTION

In this appendix a brief introduction to the design optimization, optimal control and direct transcription is given for better understanding of these concepts.

A.1 Optimal Control

A simple definition of optimal control is a design approach which seeks to identify the control design that optimizes the system objective. The cost function sought to be minimized in optimal control problems often has the form of:

$$\phi(x(t), u(t), t) = \psi(x(t_F), t_F) + \int_0^{t_F} L(x(t), u(t), t)dt \tag{A.1}$$

where $x(t)$ is the state variable trajectory, $u(t)$ is the control input trajectory, t is time, t_F is the length of the time horizon,$\psi(.)$ is the Mayer term (terminal cost) and $L(.)$ is the Lagrangian term (running cost). Constraints can also be posed on the problem, which would be discussed later. Equation A.1 is called Bolza objective if both the Mayer and Lagrangian terms exist. If $u(t)$ is the control trajectory to be optimized, the problem is called an open-loop control problem because the control input is independent of state and specified directly, whereas the control input depends on state in a feedback control system. A traditional approach to solve the optimal control problem is using the optimality conditions, such as Pontryagin's maximum principle (PMP), for finding the optimal input trajectory $u_*(t)$ which minimizes the cost function $\phi(.)$ [11, 41]. Numerical calculations are implemented in cases where the analytical solution to the boundary value problem (BVP) cannot be found or it is difficult to calculate. Methods that are based on Pontryagin's maximum principle are called indirect methods. These approaches are considered as optimize then discretize methods, since the boundary value problem found by optimality conditions is first discretized and then solved [9]. Another approach to solve the optimal control problems is the direct method. In this method the optimal control problem is first discretized and then optimized by transcription to a non-linear programming (NLP) formulation. Direct Transcription (DT) is considered as one of the discretize then optimize approaches which is also capable to solving the all at once(AAO) co-design problem [21]. We are going to elaborate more on DT in the following sections, as we will use this method to solve our problem. Before moving to the approaches for solving the co-design problem, physical system design optimization is discussed briefly.

A.2 Physical-system Design Optimization

Physical system design optimization is an attempt to achieve the optimal design which satisfies the system objectives. Design optimization can be considered as decision making process in which the decision variables are time invariant whereas in the optimal control, decision variables are time variant . In this definition, the time invariant variables are usually concerned with the physical design of a system. The compact formal statement of the optimization problem in the negative null form is:

$$
\begin{aligned}
&min f(x) \\
&g(x) \leq 0 \\
&h(x) = 0 \\
&x \in X \subseteq \mathbb{R}^n
\end{aligned}
\tag{A.2}
$$

Where x is the vector of design variables, X is the set of all possible design variables, $f(x)$ is the objective function, $g(x)$ is the inequality constraint and $h(x)$ is the equality constraint of the problem.

Now that we have described the overall definitions of optimal control and design optimization, we are going to discuss about the general methods for solving the co-design problem in the next section.

A.3 Direct Transcription

In this section we are going to discuss about the trajectory optimization using direct transcription (DT) and the application of this method in co-design. Trajectory optimization is an attempt to find the control histories that take a set of states from specified initial conditions to their desired final conditions. These control histories are to minimize an objective function that is a function of states and controls. These state are also governed by a system of first-order ordinary differential equations. In the process of optimization, algebraic path constraints for the control and state variables as well as boundary conditions should be satisfied. Objective function is:

$$
\phi(x(t), u(t), t) = \psi(x(t_F), t_F) + \int_{t_1}^{t_F} L(x(t), u(t), t) dt \tag{A.3}
$$

subject to dynamic constraints:

$$
\dot{x} = f(x(t), u(t), t) \tag{A.4}
$$

the inequality path constraints:

$$
C_{min} \leq C(x(t), u(t), t) \leq C_{max} \tag{A.5}
$$

and final conditions:

$$\eta(x(t_f), u(t_f), t_f) = 0 \tag{A.6}$$

where the initial conditions $x(t_1) = x_0$ at the fixed initial time t_1 are assigned and the final time t_f is free. To solve the optimal control problem, we should reduce the problem to a nonlinear programming problem (NLP) [22]. In other words, direct transcription, transforms infinite dimensional control design problems into finite dimensional nonlinear programming problems [3]. DT requires the continuous variables be represented (or approximated) by discrete variables, so that the problem becomes one of constrained parameter optimization problems. As a result, in DT we should first discretize the time history into N sub-intervals. The endpoints of these sub-intervals are denoted as $\{t_0, t_1, t_2, ..., t_N\}$, where t_0 is the initial time t_1 and t_N is the final timet_F as defined in equation A.3. Within each interval $[t_i, t_{i+1}]$, the time history of a solution including the numerical integration of the system equations is then approximated. The solution for dynamic constraints (eq. A.4), may be approximated using numerical integration rules such as trapezoidal integration rule:

$$\int_{t_i}^{t_{i+1}} f(t)dt = \frac{\Delta t_i}{2}[f(t_i) + f(t_{i+1})], i = 0, ..., N-1 \tag{A.7}$$

Within each sub-interval, collocation points are selected in a way to increase the accuracy of the numerical integration. The resulting integration rules are a family of modified Gaussian integration rules known as the Gauss-Lobatto rules [17]. Collocation points that maximize the power of Δt_i in the local truncation error are the roots of the corresponding Jacobi polynomial. This family of polynomials are orthogonal on the interval [−1, 1] with respect to the weight function $\omega(s) = (1-s)^\alpha(1+s)^\beta$ In particular, for the Gauss-Lobatto rules, $\alpha = \beta = 1$. A sub-interval with endpoints $[t_i, t_{i+1}]$ may be transformed to the interval [−1, 1] using the transformation $s = \frac{2(t-t_i)}{\Delta t_i} - 1$. The interpolating polynomial is formulated by interpolating $f(t)$ at the endpoints of the interval $[-1, 1]$ and at the zeros of the corresponding Jacobi polynomial.

DT can also be applied to co-design problem. Solving a co-design problem using DT is considered as a simultaneous optimization approach in which design variables are considers as time independent variables in DT. We can show this dependency in the objective function as follow:

$$\min_{d, x(t), u(t), t} \phi(d, x(t), u(t), t) \tag{A.8}$$

subject to:

$$g(d, x(t), u(t), t) \leq 0 \tag{A.9}$$

$$h(d, x(t), u(t), t) = 0 \tag{A.10}$$

$$\dot{x}(t) - f(d, x(t), u(t), t) = 0 \tag{A.11}$$

where $\phi(.)$ is the dynamic system objective function, $g(.)$is the vector of system inequality constraints, $h(.)$ is the vector of system equality constraints, $f(.)$ is the dynamic system constraints, d is the vector of design decision variables, $x(t)$ is the vector of state decision variables, $u(t)$ is the vector of input decision variables, and t is time.

Bibliography

[1] A Agarwal, ZS Filipi, DN Assanis, and DM Baker. Assessment of single-and two-zone turbulence formulations for quasi-dimensional modeling of spark-ignition engine combustion. *Combustion science and technology*, 136(1-6):13–39, 1998.

[2] Philip Langdon Alger. *Induction machines: their behavior and uses*. Gordon and Breach, 1970.

[3] James T. Allison, Tinghao Guo, and Zhi Han. Co-Design of an Active Suspension Using Simultaneous Dynamic Optimization. *Journal of Mechanical Design*, 136(8):081003–081003, June 2014.

[4] James T. Allison and Daniel R. Herber. Multidisciplinary Design Optimization of Dynamic Engineering Systems. *AIAA Journal*, 52(4):691–710, 2014.

[5] James T. Allison and Daniel R. Herber. Special Section on Multidisciplinary Design Optimization: Multidisciplinary Design Optimization of Dynamic Engineering Systems. *AIAA Journal*, 52(4):691–710, 2014.

[6] James T. Allison, Allen Kaitharath, and Daniel R. Herber. Wave Energy Extraction Maximization Using Direct Transcription. pages 485–495, November 2012.

[7] D. Assanis, G. Delagrammatikas, R. Fellini, Z. Filipi, J. Liedtke, N. Michelena, P. Papalambros, D. Reyes, D. Rosenbaum, A. Sales, and M. Sasena. Optimization Approach to Hybrid Electric Propulsion System Design. *Mechanics of Structures and Machines*, 27(4):393–421, January 1999.

[8] Le Berr, F. Le Berr, A. Abdelli, D.-M. Postariu, and R. Benlamine. Design and Optimization of Future Hybrid and Electric Propulsion Systems: An Advanced Tool Integrated in a Complete Workflow to Study Electric Devices. *Oil & Gas Science and Technology*, 67(4):17, 2012.

[9] Lorenz T. Biegler. *Nonlinear programming: concepts, algorithms, and applications to chemical processes*, volume 10. SIAM, 2010.

[10] Paul N. Blumberg, George A. Lavoie, and Rodney J. Tabaczynski. Phenomenological models for reciprocating internal combustion engines. *Progress in Energy and Combustion Science*, 5(2):123–167, January 1979.

[11] A. E. Bryson. *Applied Optimal Control: Optimization, Estimation and Control*. CRC Press, January 1975.

[12] T. A. Burress, C. L. Coomer, S. L. Campbell, L. E. Seiber, L. D. Marlino, R. H. Staunton, and J. P. Cunningham. Evaluation of the 2007 Toyota Camry Hybrid Synergy Drive System. Technical Report ORNL/TM-2007/190, Revised, Oak Ridge National Laboratory (ORNL), Oak, Ridge, TN, April 2008.

[13] Timothy A Burress, Steven L Campbell, Chester Coomer, Curtis William Ayers, Andrew A Wereszczak, Joseph Philip Cunningham, Laura D Marlino, Larry Eugene Seiber, and Hua-Tay Lin. Evaluation of the 2010 toyota prius hybrid synergy drive system. Technical report, Oak Ridge National Laboratory (ORNL); Power Electronics and Electric Machinery Research Facility, 2011.

[14] Yao Duan. Method for design and optimization of surface mount permanent magnet machines and induction machines, November 2010.

[15] Bo Egardt, Nikolce Murgovski, Mitra Pourabdollah, and Lars Johannesson Mardh. Electromobility studies based on convex optimization: Design and control issues regarding vehicle electrification. *IEEE Control Systems*, 34(2):32–49, 2014.

[16] M. Ehsani, Yimin Gao, and J.M. Miller. Hybrid Electric Vehicles: Architecture and Motor Drives. *Proceedings of the IEEE*, 95(4):719–728, April 2007.

[17] Gamal Elnagar, Mohammad A. Kazemi, and Mohsen Razzaghi. The pseudospectral Legendre method for discretizing optimal control problems. *IEEE transactions on Automatic Control*, 40(10):1793–1796, 1995.

[18] H. K. Fathy, J. A. Reyer, P. Y. Papalambros, and A. G. Ulsov. On the coupling between the plant and controller optimization problems. In *American Control Conference, 2001. Proceedings of the 2001*, volume 3, pages 1864–1869 vol.3, 2001.

[19] Hosam K. Fathy, Julie A. Reyer, Panos Y. Papalambros, and A. G. Ulsov. On the coupling between the plant and controller optimization problems. In *American Control Conference, 2001. Proceedings of the 2001*, volume 3, pages 1864–1869. IEEE, 2001.

[20] C. E. Goering and H. Cho. Engine model for mapping BSFC contours. *Mathematical and Computer Modelling*, 11:514–518, January 1988.

[21] Raphael T. Haftka. Simultaneous analysis and design. *AIAA journal*, 23(7):1099–1103, 1985.

[22] Charles R. Hargraves and Stephen W. Paris. Direct trajectory optimization using nonlinear programming and collocation. *Journal of Guidance, Control, and Dynamics*, 10(4):338–342, 1987.

[23] John B. Heywood. *Internal combustion engine fundamentals*. McGraw-Hill series in mechanical engineering. McGraw-Hill, New York, 1988.

[24] Tae-Kyung Lee and Zoran Filipi. Simulation Based Assessment of Plug-in Hybrid Electric Vehicle Behavior During Real-World 24-Hour Missions. April 2010.

[25] J. Liu and H. Peng. Modeling and Control of a Power-Split Hybrid Vehicle. *IEEE Transactions on Control Systems Technology*, 16(6):1242–1251, November 2008.

[26] Joaquim R. R. A. Martins and Andrew B. Lambe. Multidisciplinary Design Optimization: A Survey of Architectures. *AIAA Journal*, 51(9):2049–2075, 2013.

[27] R. D. Matthews, J. E. Peters, S. A. Beckel, and M. Shizhi. A new technique for thermodynamic engine modeling. *Journal of Energy*, 7:667–675, December 1983.

[28] T. J. E. Miller. Brushless permanent-magnet and reluctance motor drives. January 1989.

[29] T. J. E. Miller, A. Hutton, C. Cossar, and D. A. Staton. Design of a synchronous reluctance motor drive. *IEEE Transactions on Industry Applications*, 27(4):741–749, July 1991.

[30] TJE Miller. *Permanent Magnet and Reluctance Motor Drives*. Oxford, UK: Oxford Science Publications, 1989.

[31] Scott J. Moura. *Techniques for battery health conscious power management via electrochemical modeling and optimal control*. PhD thesis, Citeseer, 2011.

[32] Scott J. Moura, Duncan S. Callaway, Hosam K. Fathy, and Jeffrey L. Stein. Tradeoffs between battery energy capacity and stochastic optimal power management in plug-in hybrid electric vehicles. *Journal of Power Sources*, 195(9):2979–2988, 2010.

[33] Nikolce Murgovski, Lars Johannesson, Jonas Sjöberg, and Bo Egardt. Component sizing of a plug-in hybrid electric powertrain via convex optimization. *Mechatronics*, 22(1):106–120, 2012.

[34] Koichiro Muta, Makoto Yamazaki, and Junji Tokieda. Development of new-generation hybrid system ths ii - drastic improvement of power performance and fuel economy. In *SAE Technical Paper*. SAE International, 03 2004.

[35] Edward K. Nam and Robert Giannelli. Fuel consumption modeling of conventional and advanced technology vehicles in the Physical Emission Rate Estimator (PERE). *US Environmental Protection Agency*, 2005.

[36] Paul A. Nelson, K. G. Bloom, and D. W. I Dees. Modeling the performance and cost of lithium-ion batteries for electric-drive vehicles. Technical report, Argonne National Laboratory (ANL), Argonne, IL (United States), 2011.

[37] Rakesh Patil, Brian Adornato, and Zoran Filipi. Design optimization of a series plug-in hybrid electric vehicle for real-world driving conditions. *SAE Int. J. Engines*, 3(1):655–665, 2010.

[38] Rakesh M. Patil. *Combined design and control optimization: application to optimal PHEV design and control for multiple objectives*. PhD thesis, The University of Michigan, 2012.

[39] Michael A. Patterson and Anil V. Rao. GPOPS-II: A MATLAB Software for Solving Multiple-Phase Optimal Control Problems Using hp-Adaptive Gaussian Quadrature Collocation Methods and Sparse Nonlinear Programming. *ACM Trans. Math. Softw.*, 41(1):1:1–1:37, October 2014.

[40] Laura V Pérez and Elvio A Pilotta. Optimal power split in a hybrid electric vehicle using direct transcription of an optimal control problem. *Mathematics and Computers in Simulation*, 79(6):1959–1970, 2009.

[41] L. S. Pontryagin. *Mathematical Theory of Optimal Processes*. CRC Press, March 1987.

[42] Faz Rahman and Rukmi Dutta. AC Motor Control Applications in Vehicle Traction. In Fouad Giri, editor, *AC Electric Motors Control*, pages 453–486. John Wiley & Sons Ltd, 2013.

[43] Julie A. Reyer and Panos Y. Papalambros. Combined Optimal Design and Control With Application to an Electric DC Motor. *Journal of Mechanical Design*, 124(2):183–191, May 2002.

[44] G. Rizzoni, L. Guzzella, and B. M. Baumann. Unified modeling of hybrid electric vehicle drivetrains. *IEEE/ASME Transactions on Mechatronics*, 4(3):246–257, September 1999.

[45] Aymeric Rousseau, Sylvain Pagerit, and David Wenzhong Gao. Plug-in Hybrid Electric Vehicle Control Strategy Parameter Optimization. *Journal of Asian Electric Vehicles*, 6(2):1125–1133, 2008.

[46] Ä°smet Sezer and Atilla Bilgin. Mathematical analysis of spark ignition engine operation via the combination of the first and second laws of thermodynamics. *Proceedings of the Royal Society of London A: Mathematical, Physical and Engineering Sciences*, 464(2100):3107–3128, December 2008.

[47] Shashi K. Shahi, G. Gary Wang, Liqiang An, Eric Bibeau, and Zhila Pirmoradi. Using the Pareto Set Pursuing Multiobjective Optimization Approach for Hybridization of a Plug-In Hybrid Electric Vehicle. *Journal of Mechanical Design*, 134(9):094503–094503, August 2012.

[48] Ching-Shin Norman Shiau, Nikhil Kaushal, Chris T. Hendrickson, Scott B. Peterson, Jay F. Whitacre, and Jeremy J. Michalek. Optimal Plug-In Hybrid Electric Vehicle Design and Allocation for Minimum Life Cycle Cost, Petroleum Consumption, and Greenhouse Gas Emissions. *Journal of Mechanical Design*, 132(9):091013–091013, September 2010.

[49] Wen Liang Soong. *Design and modelling of axially-laminated interior permanent magnet motor drives for field-weakening applications.* Ph.D., University of Glasgow, 1993.

[50] F. U. Syed, M. L. Kuang, J. Czubay, and H. Ying. Derivation and Experimental Validation of a Power-Split Hybrid Electric Vehicle Model. *IEEE Transactions on Vehicular Technology*, 55(6):1731–1747, November 2006.

[51] Wang Tiecheng, Zheng Ping, Zhang Qianfan, and Cheng Shukang. Design characteristics of the induction motor used for hybrid electric vehicle. In *2004 12th Symposium on Electromagnetic Launch Technology, 2004*, pages 523–527, May 2004.

[52] J Van Mierlo. Models of energy sources for EV and HEV: fuel cells, batteries, ultracapacitors, flywheels and engine-generators. *Journal of Power Sources*, 128(1):76–89, March 2004.

[53] Andreas Wächter and Lorenz T Biegler. On the implementation of an interior-point filter line-search algorithm for large-scale nonlinear programming. *Mathematical programming*, 106(1):25–57, 2006.

[54] Nansi Xue, Wenbo Du, Thomas A. Greszler, Wei Shyy, and Joaquim R. R. A. Martins. Design of a lithium-ion battery pack for PHEV using a hybrid optimization method. *Applied Energy*, 115:591–602, February 2014.

[55] H. Lin Y Zhang. Performance modeling and optimization of a novel multi-mode hybrid powertrain. *Journal of Mechanical Design*, 128:79, 2006.